Showcasing research from University of Toulouse III, France, with contribution of University of Wien, Austria.

Dinuclear tricarbonylrhenium(I) complexes: impact of regioisomerism on the photoluminescence properties

Two isomeric dinuclear tricarbonylrhenium(I) complexes were compared with each other and with the parent mononuclear compound. The dimer photoluminescence was sensitive to mechanical stimuli. The positional isomerism influenced the amplitude of this effect, as well as the aggregation-induced emission (AIE) properties.

The authors are grateful to Ms. Cécily Noaillac for the gift of the beautiful background photo.

As featured in:

See Florence Bedos-Belval, Suzanne Fery-Forgues *et al.*, *Dalton Trans.*, 2024, **53**, 16512.

ROYAL SOCIETY OF CHEMISTRY

rsc.li/dalton

Registered charity number: 207890

Dalton Transactions

ROYAL SOCIETY OF CHEMISTRY

PAPER

View Article Online
View Journal | View Issue

Cite this: *Dalton Trans.*, 2024, **53**, 16512

Dinuclear tricarbonylrhenium(I) complexes: impact of regioisomerism on the photoluminescence properties†

Stéphen Le Garrec, [a] David Martins-Bessa, [a] Mariusz Wolff, [b,c] Béatrice Delavaux-Nicot, [d] Sonia Mallet-Ladeira, [e] Charles-Louis Serpentini, [f] Eric Benoist, [a] Florence Bedos-Belval *[a] and Suzanne Fery-Forgues *[a]

Dinuclear Re(I) complexes have proportionally been much less studied than mononuclear analogues. In particular, very little information is available about their solid-state emission properties. In this work, two structural isomers of dinuclear complexes (**Bi-Re-*meta*Phe** and **Bi-Re-*para*Phe**), which differ by the relative position of the coordination spheres on a central phenyl ring, were synthesized and compared with each other and with the parent mononuclear compound (**Mono-Re-Phe**), from a theoretical and experimental point of view. In solution, the electronic, electrochemical and spectroscopic properties of the dinuclear complexes were almost identical, and rather close to those of the monomer. In the solid state, the photoluminescence (PL) efficiency of dimers was not higher than that of the monomer, but a clear mechanoresponsive luminescence (MRL) effect appeared only for the former ones. The positional isomerism influenced the amplitude of this effect, as well as the aggregation-induced emission (AIE) properties in a water-acetonitrile mixture. This study reveals the importance of positional isomerism to modulate the emission properties in the solid state. It also shows the advantage of dinuclear structures to access new MRL-active materials.

Received 2nd July 2024,
Accepted 23rd August 2024

DOI: 10.1039/d4dt01907e

rsc.li/dalton

Introduction

Over the last two decades, tricarbonylrhenium(I) complexes have attracted significant attention due to their stability, very low toxicity and attractive spectroscopic properties, which made them popular bio-imaging agents and sensors.[1] Their coordination chemistry is clearly dominated by mononuclear species. However, many examples of complexes incorporating two rhenium centers have been reported. They can be divided into two categories. Some have little or no electronic conjugation between the coordination spheres. They can be seen as covalent assemblies of mononuclear complexes, whose physicochemical properties are the sum of the properties of each fragment and the linker. This makes them valuable probes for precise targeting in imaging microscopy,[2,3] as well as potential candidates in the fields of anticancer drugs[4–7] and photodynamic therapy,[8] anion detection,[9] liquid crystals,[10] and photocatalysis.[11,12] The second type of complex is characterized by the electronic conjugation between the two metal centers through an organic ligand. This allows the emergence of new chemotherapeutic properties.[13,14] New electrochemical and spectroscopic properties also appear,[15–23] which may be of interest for applications such as organic catalysis,[24–27] electrochemical devices,[28,29] sensing,[30] and bio-imaging.[28,31–33] For photochemically-active complexes, the photoproduction of species like $^1O_2$ and CO is also increased with respect to mononuclear species.[34–36] From a general point of view, the spectroscopic properties of dinuclear tricarbonylrhenium(I) complexes in solution attract more and more attention, although they are probably much less studied than those of luminescent iridium

[a]*SPCMIB, CNRS UMR 5068, Université de Toulouse III Paul Sabatier, 118 route de Narbonne, 31062 Toulouse cedex 9, France. E-mail: florence.bedos@univ-tlse3.fr, suzanne.fery-forgues@univ-tlse3.fr*
[b]*Institut für Funktionelle Materialien und Katalyse, Universität Wien, Währinger Straße 38-42, 1090 Wien, Austria*
[c]*Institute of Chemistry, University of Silesia in Katowice, Szkolna 9th Street, 40-006 Katowice, Poland*
[d]*Laboratoire de Chimie de Coordination, CNRS (UPR 8241), Université de Toulouse (UPS, INPT), 205 route de Narbonne, 31077 Toulouse Cedex 4, France*
[e]*Service Diffraction des Rayons X, Institut de Chimie de Toulouse, ICT-UAR 2599, Université de Toulouse III Paul Sabatier, 118 route de Narbonne, 31062 Toulouse cedex 9, France*
[f]*Laboratoire SOFTMAT, CNRS UMR 5623, Université de Toulouse III Paul Sabatier, 118 route de Narbonne, 31062 Toulouse cedex 9, France*

†Electronic supplementary information (ESI) available: Experimental details including NMR, HRMS and IR spectra, molecular views and crystallographic data, theoretical calculations, electrochemical experiments, photoluminescence spectra and decays. CCDC 2365135–2365138. For ESI and crystallographic data in CIF or other electronic format see DOI: https://doi.org/10.1039/d4dt01907e

complexes,[37–43] for example. Regarding specifically the solid-state emission properties, which are highly sought after for applications in the field of photoluminescent materials, biosensing and security devices,[44–48] only some rare dinuclear tricarbonylrhenium(I) complexes have been reported to date.[16,17,49,50] However, significant variations compared to mononuclear complexes can be expected, due to the modified electron system and to a change in the solid-state molecular arrangement and intermolecular bonds, which play a major role in photoluminescence (PL).[51]

Recently, our team has developed original mononuclear tricarbonylrhenium(I) complexes that are potentially useful for applications in the field of photoluminescent materials.[52–59] Besides strong solid-state luminescence enhancement (SLE)[51] and aggregation-induced emission (AIE)[60] effect, some of them showed unprecedented mechanoresponsive luminescence (MRL) properties.[56–59] In the present work, the structure of one of the best performing complexes (**Re-Phe**, Fig. 1) based on the (3-(2-pyridyl)-1,2,4-triazole) (pyta) ligand, has been selected. The analogous mononuclear complex **Mono-Re-Phe**, in which an alkyl chain was introduced for solubility reasons, and the new dinuclear tricarbonylrhenium(I) complexes (**Bi-Re-*para*Phe** and **Bi-Re-*meta*Phe**) merging two of these units were designed and synthesized (Fig. 1). The two dimers differ by the position of their pyta moieties on the central phenyl ring. The comparison with parent mononuclear complex **Mono-Re-Phe** allowed to better understand the influence of the dinuclear structure on their electronic, electrochemical and spectroscopic properties. Moreover, subtle changes in molecular geometry and intermolecular interactions in the solid state can be expected between the dimers, possibly resulting in new physicochemical properties. The impact of regioisomerism upon the PL properties was therefore specifically investigated. To the best of our knowledge, such a study is unprecedented in the literature. No example of *cis*/*trans* positional isomerism with respect to a photoswitchable double bond was found either, while such changes have been reported to govern the spectroscopic behavior of mononuclear species.[61,62] In a somewhat distant area, it has been shown that *cis*/*trans* conformational isomerism has no effect on the photocatalytic properties of an anthracene-based dinuclear Re(I) complex in solution.[36] Studies dealing with the diastereoisomerism of anticancer dinuclear Re(I) complexes incorporating chiral centers are still rare and clearly belong to another field of research.[14] The present study revealed that our three complexes in solution show rather conventional behavior. In contrast, in the solid-state, unpredictable MRL properties emerged only for dimers, while regioisomerism allowed the emission efficiency and AIE properties to be modulated. This is the first study in this field, and it could open the door to a variety of new multimetallic complexes.

Results and discussion

Synthesis and characterization

The procedure used to synthesize the three new complexes is described in Scheme 1. The meaning of abbreviations is reported in the ESI, and the chemical characterization of the compounds is given in the Experimental section. In brief, picolinohydrazide was reacted with nonanoic acid in the presence of HATU to afford the oxadiazole derivative. The latter was then condensed with aniline or the relevant phenylenediamine in the presence of a catalytic amount of *p*-TsOH in refluxing 1,2-dichlorobenzene to give the corresponding ligands **L-Phe**, **L-*para*Phe** and **L-*meta*Phe** respectively, with a fair to good yield after purification. The ligands were then reacted with [Re(CO)$_5$Cl] in refluxing methanol to afford the corresponding tricarbonylrhenium(I) complexes in good yields (83%, 76% and

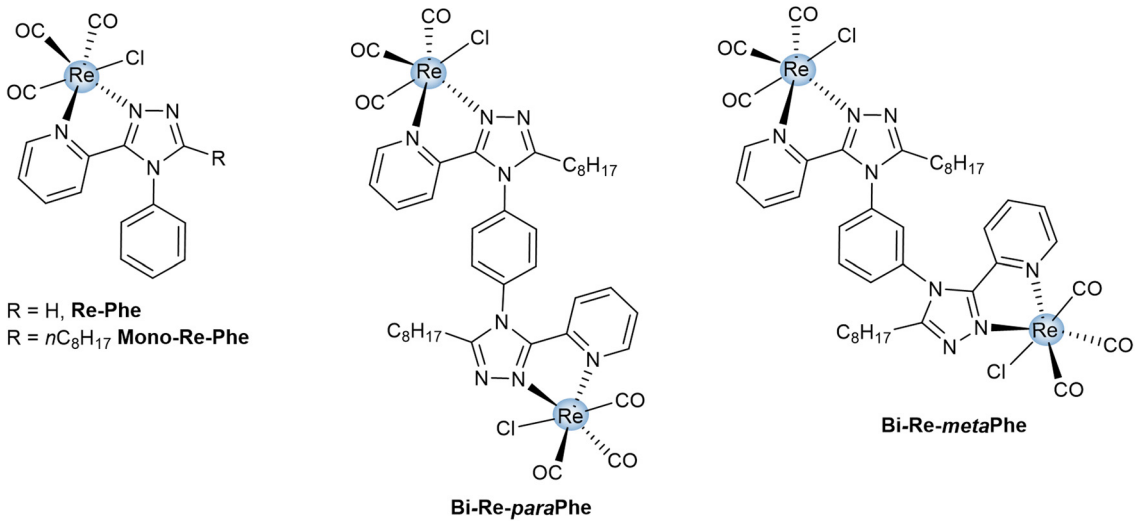

Fig. 1 Chemical structures of dimeric complexes **Bi-Re-*para*Phe** and **Bi-Re-*meta*Phe**, and reference monomeric complexes **Re-Phe** and **Mono-Re-Phe**.

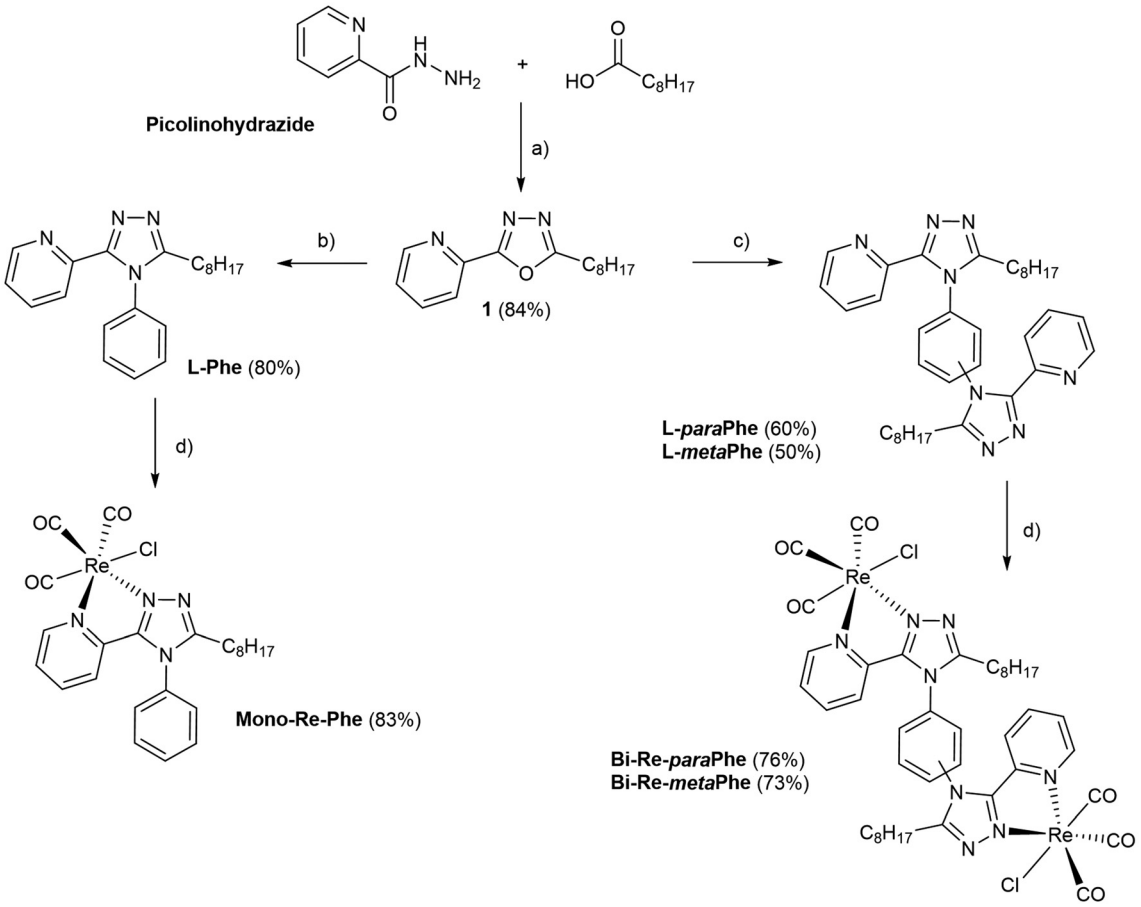

Scheme 1 Synthesis of complexes **Mono-Re-Phe**, **Bi-Re-*para*Phe** and **Bi-Re-*meta*Phe**. Conditions and reagents: (a) DIPEA, HATU, acetonitrile, 6 h, r.t.; and then DIPEA, *p*-TsCl, 16 h, r.t. (b) Aniline, *p*-TsOH, 1,2-dichlorobenzene, 20 h, 180 °C. (c) Phenylenediamine, *p*-TsOH, 1,2-dichlorobenzene, 20 h, 180 °C. (d) $[Re(CO)_5Cl]$, methanol, 16 h, 65 °C.

73%, for **Mono-Re-Phe**, **Bi-Re-*para*Phe** and **Bi-Re-*meta*Phe**, respectively).

All synthesized molecules were characterized by ^1H and ^{13}C NMR spectroscopy, high resolution mass spectrometry and infrared spectroscopy (Fig. S1–23†). The purity of the complexes was checked by elemental microanalysis. It is noteworthy that for the dimeric complexes **Bi-Re-*para*Phe** and **Bi-Re-*meta*Phe**, the NMR signals corresponding to the H3 and H4 pyridine protons were split (Fig. S16 and 19†). This indicates the presence of at least two conformers, the identification of which is the topic of a forthcoming publication.

Crystal structures

X-Ray quality crystals of complexes **Mono-Re-Phe** and **Bi-Re-*meta*Phe** were grown at the interface of a chloroform solution topped with pentane, and from slow evaporation of a DCM solution, respectively. No suitable crystal could be obtained from the **Bi-Re-*para*Phe** complex. However, crystals of ligands L-***para*Phe** and L-***meta*Phe**, grown from slow evaporation of acetone and acetone/CH_2Cl_2 solutions, respectively, were examined to get an idea of the molecular conformation. The crystallographic data of **Re-Phe**[57] were further processed (Fig. S24–27 and Comment S1†) and used for comparison. Selected crystallographic data are collected in the Experimental section and in Tables S1 and 2.†

The coordination spheres of complexes **Mono-Re-Phe** and **Bi-Re-*meta*Phe** exhibit a quasi-octahedral geometry (Fig. 2). Distortion parameters are listed in Tables S3 and 4.† The rhenium atom is coordinated to three carbonyl groups in a *fac* configuration, one chlorine atom, the pyridyl N1 atom and the triazole N2 atom. For **Bi-Re-*meta*Phe**, the geometry of both metallic centers is exactly the same. Distances and angles of the coordination spheres are close to those found for this type of complexes. The pyridyl-triazole moieties are almost planar. The phenyl ring is close to orthogonal with respect to the pyta moiety, with a dihedral α angle of 82.6° for **Mono-Re-Phe** (more pronounced than for the analogue deprived of the alkyl chain ($\alpha \sim 68°$)[57]), and two identical α angles of 81.9° for **Bi-Re-*meta*Phe**. It must be noted that for the latter complex, the crystal obtained represents only one of the possible conformations, where the two pyta moieties face each other in an antisymmetric way, each being arranged orthogonally with respect to the central phenyl ring. This doubly-twisted conformation was visible on the structure of ligand L-***meta*Phe**,

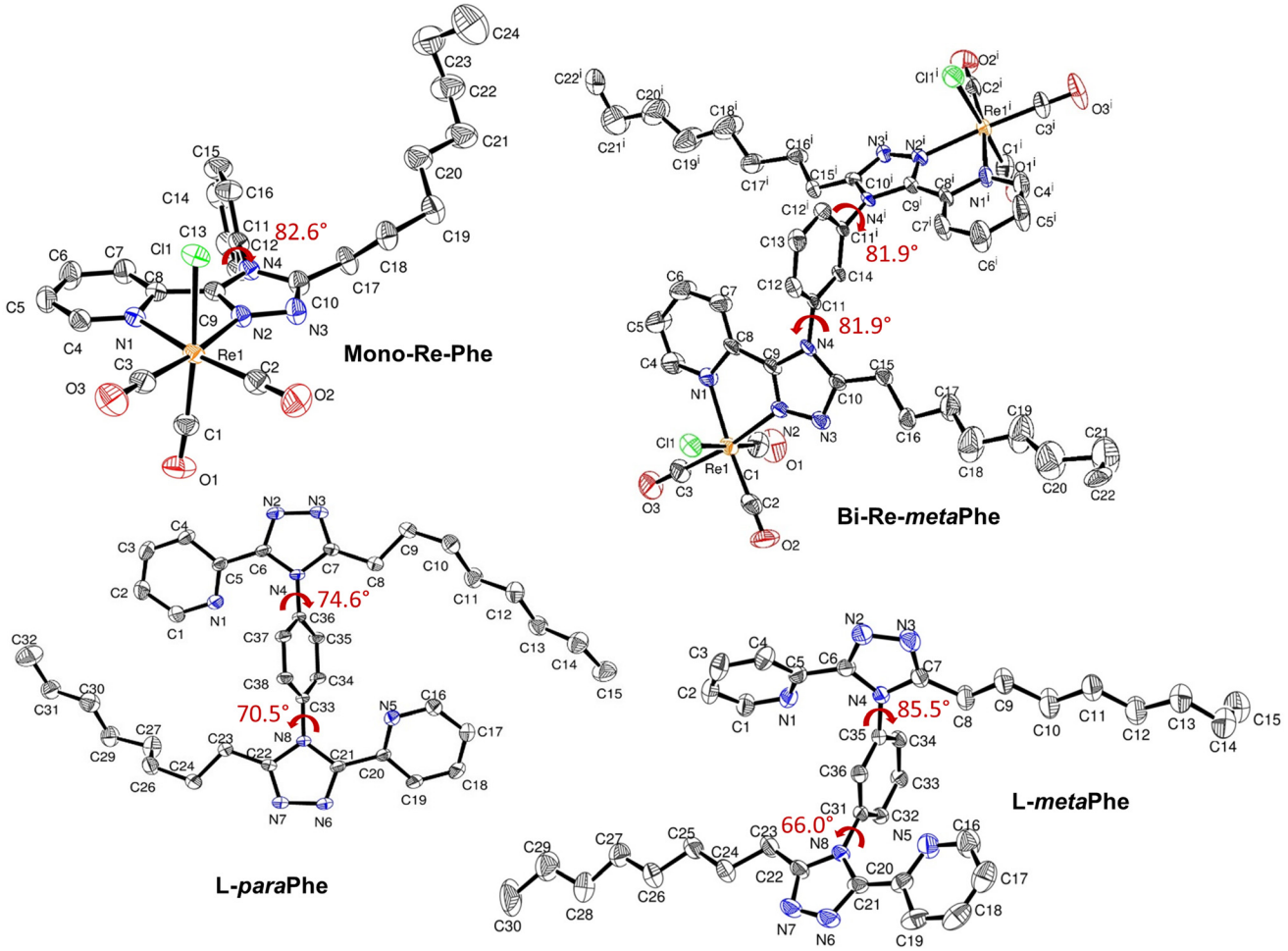

Fig. 2 Molecular structures of complexes **Mono-Re-Phe** and **Bi-Re-*meta*Phe**, and ligands L-***para*Phe** and L-***meta*Phe**, with the dihedral angle α indicated in red ink. Hydrogen atoms are not represented for the sake of clarity. Displacement ellipsoids are drawn at 50% probability. Symmetry code for **Bi-Re-*meta*Phe**: (i) $1 - x, y, \frac{1}{2} - z$.

where the triazole rings of the two molecules form distinct α angles of 85.5° and 66.0° (81.3° and 68.2° for the second molecule of the cell). The examination of the crystal structure of ligand **L-*para*Phe** also shows that the triazole rings form α angles of 70.5° and 74.6° with the central phenyl ring. According to DFT calculations (*vide infra*), the torsion angles in **Bi-Re-*para*Phe** in solution should be close to orthogonal (Table S12†). So, in the absence of X-ray data, it can be assumed that a doubly twisted conformation is retained for the **Bi-Re-*para*Phe** complex.

For complex **Mono-Re-Phe**, two enantiomers, which differ by the position of the organic ligand with respect to the chlorine atom, coexist in the crystal cell in identical proportions. The same is true for **Bi-Re-*meta*Phe**, each molecule of which is constituted by two enantiomers of the same type. Both crystal structures are stabilized by C–H···O and C–H···Cl short contacts, which can be considered as weak hydrogen bonds (Fig. 3, Table S5†). Additionally, both structures show C–H···π interactions (Table S6†), but no obvious π–π stacking interactions were detected, contrary to what was observed for **Re-Phe** (Table S7†). This comparison shows the value of the alkyl chain to separate the aromatic moieties. More precisely, as regards the whole arrangement, molecules of **Mono-Re-Phe** are displayed on four distinct planes, with opposite orientations (Fig. S28†). Two neighboring molecules in the antiparallel arrangement form cyclic dimers $R_2^2(12)$ through C5–H5(pyr)···Cl1 interactions, which are further connected through C16–H16(Phe)···O1(CO) interactions to afford a 2D network along the *ab* plane (Fig. 3a and S29†). Regarding **Bi-Re-*meta*Phe**, all molecules are aligned along the same direction (Fig. S30†). They form antiparallel dimers (Fig. S30b†). Strong C7–H7(pyr)···π(Phe) (Fig. S31†) and N3(trz)···H12(Phe) interactions are detected between neighboring molecules. Remarkably, the presence of the alkyl chain and DCM molecules play an important role in structuring the network. Molecules of **Bi-Re-*meta*Phe** connect *via* intermolecular C22–H22A$(CH_3)_{octyl}$···O3(CO) interactions along the *ab* plane. One DCM molecule is connected to two molecules of complex *via* intermolecular C15–H15B$(CH_2)_{octyl}$···Cl2 and C22–H22B$(CH_3)_{octyl}$···Cl3 interactions forming an infinite 1D ladder chain which propagates

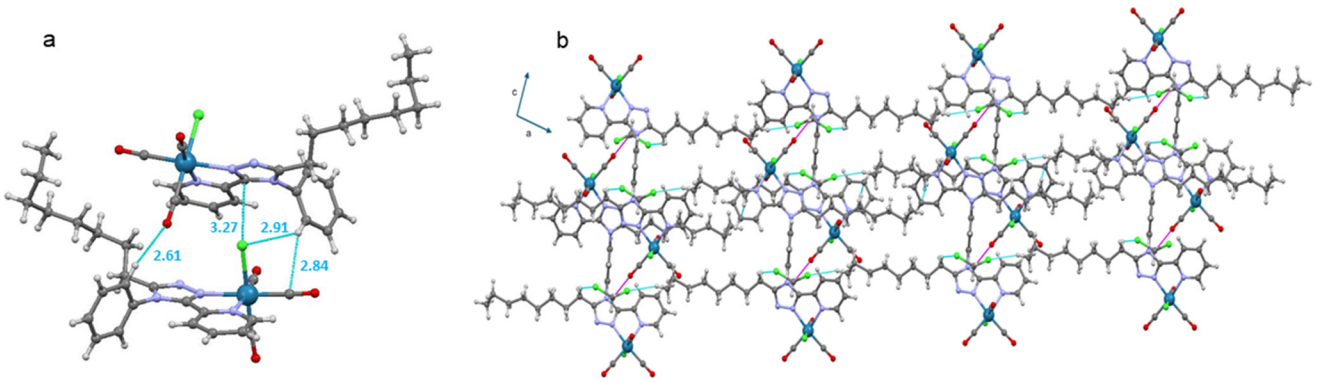

Fig. 3 (a) Molecular view of **Mono-Re-Phe** with distances of short contacts in Å. (b) Representation of one-dimensional chains and two-dimensional network in **Bi-Re-*meta*Phe** formed by connection of molecules through DCM (in an up/down–up/down fashion) *via* intermolecular C15–H15B$(CH_2)_{octyl}$···Cl2(DCM) and C22–H22B$(CH_3)_{octyl}$···Cl3(DCM) interactions (cyan color), and C23–H23B(DCM)···O2(CO) interactions (magenta color).

along the *ac* plane. The same DCM molecule is also connected to a third molecule of complex through intermolecular C23–H23B(DCM)···O2(CO) interactions, leading to a 2D network (Fig. 3b). It can be anticipated that molecules of **Bi-Re-*meta*Phe**, which arrange as layers, have more facility to glide on each other upon mechanical forces than those of **Mono-Re-Phe**, the packing of which is much denser.

The analysis of Hirshfeld surfaces (HS)[63] was performed to visualize and quantify the intermolecular interactions in the crystal lattice of complexes **Re-Phe**, **Mono-Re-Phe** and **Bi-Re-*meta*Phe**. In Fig. 4a–c, where HS are plotted over d_{norm}, the red spots represent the regions of the surface where intermolecular contacts are strong, and the blue areas illustrate the domains where neighboring atoms are too far away to interact with each other. It can be seen that the red regions concentrate on the part of the fat chain close to triazole ring for **Mono-Re-Phe** (Fig. 4b) and **Bi-Re-*meta*Phe** (Fig. 4c), while they are distributed more homogeneously on the surface of **Re-Phe** (Fig. 4a). On the shape-index representation (Fig. 4d), blue triangles represent the convex regions formed by carbon atoms present in the molecule inside the surface, while red triangles represent concave regions due to the carbon atoms of the

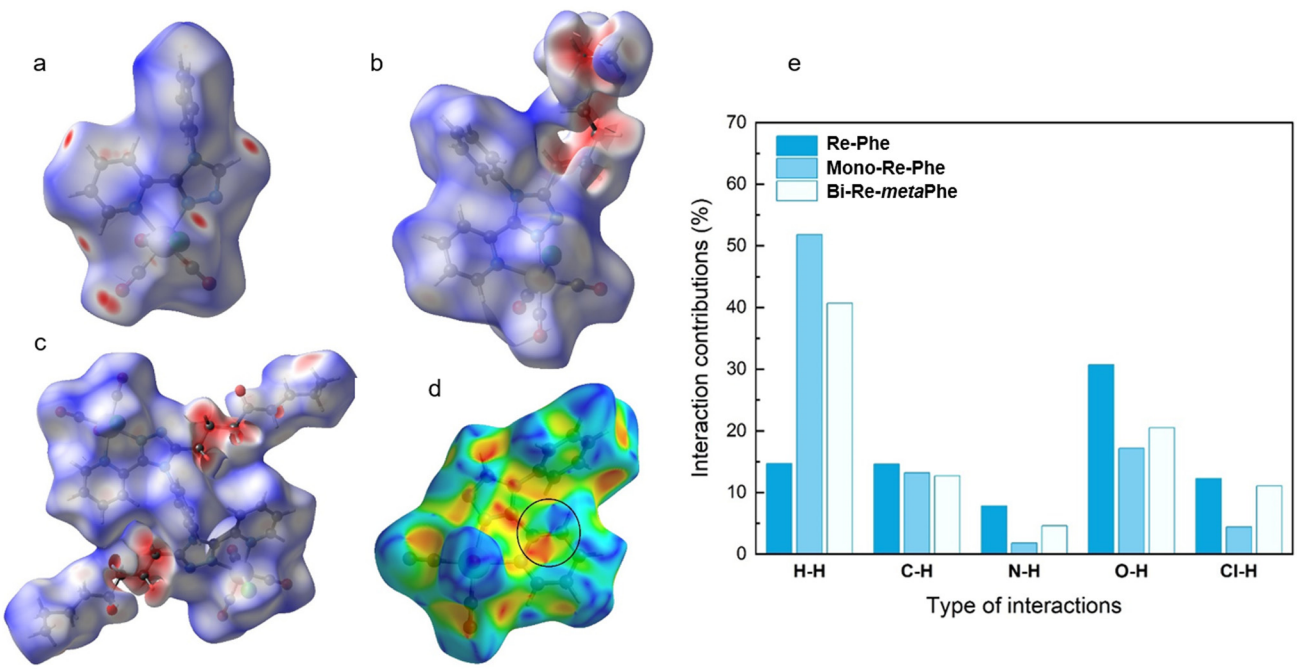

Fig. 4 (a–c) Hirshfeld surfaces (HS) plotted over d_{norm} for **Re-Phe** (a), **Mono-Re-Phe** (b) and **Bi-Re-*meta*Phe** (c). (d) HS plotted over shape index for **Re-Phe** with adjacent triangles revealing the π–π stacking surrounded by the black circle. (e) Percentage contributions of different interactions to the HS for the three complexes.

π-stacked molecule above it. Adjacent red and blue triangles that highlight π–π stacking interactions were only observed for **Re-Phe**. The percentage contributions of different interactions to the HS were quantified (Fig. S32–34 and Comment S2†) and compared (Fig. 4e). This approach confirms that the number of intermolecular interactions involving the aromatic moieties was decreased in the presence of the alkyl chain.

Electronic properties

Computational studies were made using the density functional theory (DFT) and time-dependent DFT (TD-DFT) methods considering the complexes in dichloromethane continuum (Tables S8–25,† Fig. 5 and Fig. S35–41†). Calculations were repeated for **Re-Phe** so that the data were fully comparable with those of the new complexes. As expected, the alkyl chain has little influence on the electronic properties and complexes **Re-Phe** and **Mono-Re-Phe** are very similar, so that only the latter one was discussed below. For **Mono-Re-Phe** and **Bi-Re-*meta*Phe**, the calculated bond lengths and angles were in excellent agreement with the X-ray experimental data (Tables S8 and 9†). It is also the case for the FT-IR spectra of all complexes (Fig. S41†). The composition of the frontier molecular orbitals (Tables S14–16, and Fig. S35–38†) revealed that the electronic density of the three highest occupied molecular orbitals (HOMO, H−1 and H−2) of **Mono-Re-Phe** is localized on the rhenium atom and carbonyl ligands, as well as on the chlorine atom for the two first ones, as is commonly the case for tricarbonylrhenium(I) complexes. This electronic distribution was also found for orbitals HOMO to H−5 of the dinuclear Re complexes. Regarding the lowest unoccupied molecular orbitals, the LUMO and L+1 of the three complexes are centered on the pyta moiety. Significant differences between the three complexes appear for upper and lower orbitals. For instance, the electronic density of L+2 is almost totally concentrated on the phenyl ring of **Mono-Re-Phe** (96%), while it is distributed between the phenyl ring and the pyta moiety of **Bi-Re-*para*Phe** (87/12) and **Bi-Re-*meta*Phe** (66/34). Regarding the energy levels, the HOMO–LUMO gap was slightly decreased when passing from **Mono-Re-Phe** (4.03 eV), to **Bi-Re-*para*Phe** (3.98 eV), and then to **Bi-Re-*meta*Phe** (3.96 eV). The HOMO, H−1 and H−2 of the dinuclear complexes have very close energy levels, as well as H−4 and H−5, and this is also the case for their LUMO and L+1. Actually, these orbitals are almost degenerate with a very small energy difference due to the symmetric arrangement of the complexes. In contrast, for the mononuclear compound, these energy levels vary more importantly.

For the three complexes, the lowest energy transitions correspond to a shift of the electronic density from the coordination sphere to the organic ligand (Tables S18–20†). They are therefore of metal-to-ligand charge transfer (MLCT), halogen-to-ligand charge transfer (XLCT) and ligand-to-ligand charge transfer (LLCT) type. The most significantly-active transitions are H−1 → LUMO at 382.8 nm for **Mono-Re-Phe**, H−3 → L+1/H−2 → L (389.6 nm) for **Bi-Re-*meta*Phe**, and H−3 → L/H−2 → L+1 (388.7 nm) for **Bi-Re-*para*Phe**. Many high-energy transitions are of intra-ligand and ligand-to-ligand charge transfer (ILCT/LLCT) type. It is noteworthy that the most active transitions involve orbitals that are very similar for the three complexes.

The natural population analysis (NPA) (Table S24†) showed that the calculated charge on the rhenium atoms is −0.99(*e*) whatever the complex. The positively charged carbon atoms of the carbonyl ligands accept as much as ∼0.74/0.77/0.76(*e*) from the Re atoms, while the negatively charged nitrogen atoms N(1), N(2) and chlorine atom Cl(1) donate as much as ∼0.39(*e*), ∼0.23(*e*) and ∼0.46(*e*) to Re atoms, respectively. In summary, the mono and bimetallic complexes are very close from an electronic point of view, and great similarities can be expected in the experimental properties in solution.

Electrochemistry

The electrochemical behavior of the new complexes was studied by cyclic voltammetry (CV) and Osteryoung square wave voltammetry (OSWV) measurements in dichloromethane at room temperature. The results are displayed in Table 1, Fig. 6 and Fig. S42–53.† The **Mono-Re-Phe** complex had the electrochemical characteristics of a Re(I) chlorotricarbonyl compound with a (3-(2-pyridyl)-1,2,4-triazole) substituted in the N position by a phenyl group in an orientation almost perpendicular to the pyta ligand (Table 1). Indeed, comparison with its bidentate ligand and its non-alkyl-substituted counterpart allowed us to clearly attribute its first oxidation process to a monoelectronic oxidation process centered on the Re(I) moiety, and its first reduction process to that of its substituted pyta moiety. Moreover, the value of the latter process situated at −1.39 V was around 100 mV more cathodic than that of complex **Re-Phe**,[57] indicating the influence of the electron-donating alkyl group. In contrast, the Re center was not very sensitive to this change, while a E_1^{ox}/E_1^{red} intensity ratio of 1 was well observed in CV at 0.2 V s^{-1} as for **Re-Phe** (Fig. 6a).

Remarkably, the two bimetallic rhenium complexes presented the same electrochemical signatures. In OSSW, in the anodic part, two irreversible oxidation processes were observed. The first one was clearly assigned to the oxidation of both Re centers whose potential value (1.43 V) is very close to that of the mononuclear compounds. No electronic communication was detected between these metallic centers which behave as independent redox centers. In CV, a broad peak was observed for the reduction of the pyta moieties, and further examination of this process by OSWV allowed the detection of two very close reduction processes of equal intensity centered at −1.29 V, whatever the experimental conditions (Fig. 6b and Fig. S48†). Globally, in reduction, the bimetallic complexes are less electron rich than their mononuclear counterpart. Their reduction potential is characteristic of a preferred perpendicular arrangement of their pyta moieties with the central phenyl ring, as already observed in this family of complexes,[52,53,56–58] and confirmed by X-ray study. The splitting of the reduction process by around 70 mV is likely due to the presence of the two possible enantiomers in *syn* and *anti*-conformations as

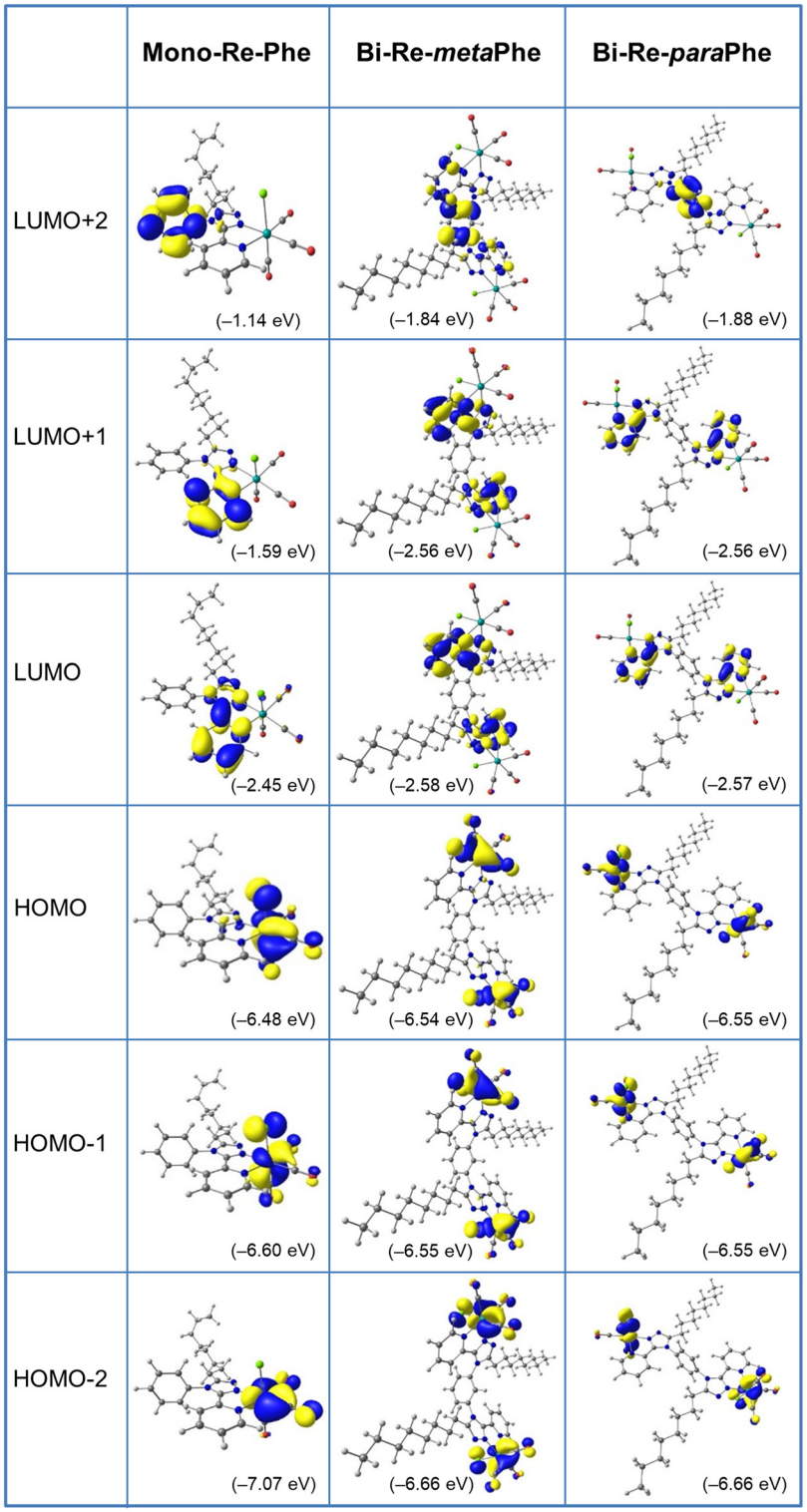

Fig. 5 Isodensity plots (isovalue = 0.03 e bohr^{-3}) and energy levels of the first frontier molecular orbitals, for complexes **Mono-Re-Phe**, **Bi-Re-*para*Phe**, and **Bi-Re-*meta*Phe** in dichloromethane, according to DFT calculations at the PBE1PBE/LANL2DZ level of theory.

already mentioned in the literature for other tricarbonylrhenium(I) derivatives.[64–66]

For the bimetallic complexes, exhaustive electrolyses in reduction mainly led to decomposition reactions. In contrast, those performed at the potential of the first oxidation process allowed the quantification of a possible two-electron oxidation process. Interestingly, in CVs, comparison of the intensity of their redox processes with those of **Mono-Re-Phe** clearly

Table 1 Selected electrochemical data of complexes **Mono-Re-Phe**, **Bi-Re-*para*Phe**, **Bi-Re-*meta*Phe**, and their respective ligands, L-**Phe**, L-***para*Phe**, L-***meta*Phe**, at 10^{-3} M. Values determined by OSWV on a Pt working electrode in CH_2Cl_2 + 0.1 M $n[Bu_4][NBF_4]$ at room temperature.[a,b] Ferrocene was used as internal reference

	Oxidation		Reduction		
	E_2	E_1	E_1	E_2	E_3
Re-Phe[c]	1.78	1.46	−1.29[d]	−1.78	
L-**Phe**	1.99	1.70	—	—	—
Mono-Re-Phe	1.75	1.44	−1.39[e]	—	
L-***para*Phe**	—	1.70	—	—	—
Bi-Re-*para*Phe	1.75	1.43	−1.24[f]	−1.33[f]	−1.88[g]
L-***meta*Phe**		1.70[h]	—	—	—
Bi-Re-*meta*Phe	1.75	1.43	−1.24[f]	−1.34[f]	−1.88[g]

[a] OSWVs were obtained using a sweep width of 20 mV, a frequency of 20 Hz, and a step potential of 5 mV. [b] Potential values in Volts *vs.* SCE (Fc^+/Fc is observed at 0.55 V ± 0.01 V *vs.* SCE). [c] From ref. 57. [d] One-electron quasi-reversible process at 1.0 V s^{-1}. [e] More reversible process at 10 V s^{-1} (Fig. S44†), with a 1/1 intensity ratio for E_1^{ox}/E_1^{red} at 0.2 V s^{-1} (Fig. S43 right†). [f] Two close reduction processes in 1/1 intensity ratio whatever the SW rate conditions (Fig. S48†). These processes give one more reversible process at 50 V s^{-1} in CV (Fig. S47†). [g] Very small intensity process. [h] Ill defined (Fig. S52†).

highlighted their difference and confirmed the number of electrons involved in their respective redox processes (Fig. 6a).

It is noteworthy that the dimerization of the mononuclear compound using its phenyl moiety as connected unit in *meta* or *para* position had more impact on its reduction potential (or on its LUMO energy level) than on its oxidation potential (or on its HOMO energy level). These results are in total agreement with theoretical data. Indeed, for the three compounds, the HOMO on one hand, and the LUMO on the other hand, are of similar nature. Moreover, the value of the energy level of the respective HOMOs is nearly the same (±0.07 eV), and that of the LUMOs is also close (±0.12 eV). In comparison with the mononuclear compound, a slight stabilization of these orbitals is observed when forming the dinuclear compounds leading to a smaller energy gap, as clearly highlighted experimentally by electrochemistry.

Finally, the values of the electrochemical HOMO–LUMO gap (E_g^{el}) found experimentally for **Mono-Re-Phe** and the two bimetallic complexes, around 2.55 eV, 2.46 and 2.46 eV, respectively, also fit very well with the calculated E_{calc} gap values 2.67, 2.62 and 2.62 eV, highlighting good correlations with the theoretical study (Table S26†).

UV-visible absorption and emission properties

The three complexes in dilute dichloromethane solutions were very pale yellow in daylight. Their absorption spectra (Fig. 7 and Table 2) showed intense bands between 200 and 300 nm, attributed to a combination of ILCT and MLCT transitions. At low-energy, a band of moderate intensity with MLCT character peaked around 379 nm for **Mono-Re-Phe** and above 391 nm for **Bi-Re-*para*Phe** and **Bi-Re-*meta*Phe**. With respect to the monomer, the molar extinction coefficient of the dimers was multiplied by a little more than two, because of the two chromophoric units and the extension of the electron conjugated system due to the linker.

When illuminated by UV light (365 nm), the three complexes in dichloromethane solutions emitted weak orange-red light. The emission spectra showed a single unresolved band, peaking around 616 nm for the **Mono-Re-Phe** complex and ~636 nm for the dimers. The experimental emission maxima were only slightly below those calculated by TD-DFT and DFT (Table S22†), considering the involvement of the lowest ^{3}MLCT state. Emission decays were monoexponential (Fig. S54†). The lifetimes, around 114 ns for the monomer and 72 ns for the dimers, confirmed that emission is due to phosphorescence. The quantum yields were moderate, in the 2×10^{-2} range, and were increased by 64%, 24% and 16% for **Mono-Re-Phe**, **Bi-Re-*para*Phe** and ***Bi*-Re-*meta*Phe**, respectively, when passing from aerated to argon-bubbled solutions. The bimetallic complexes

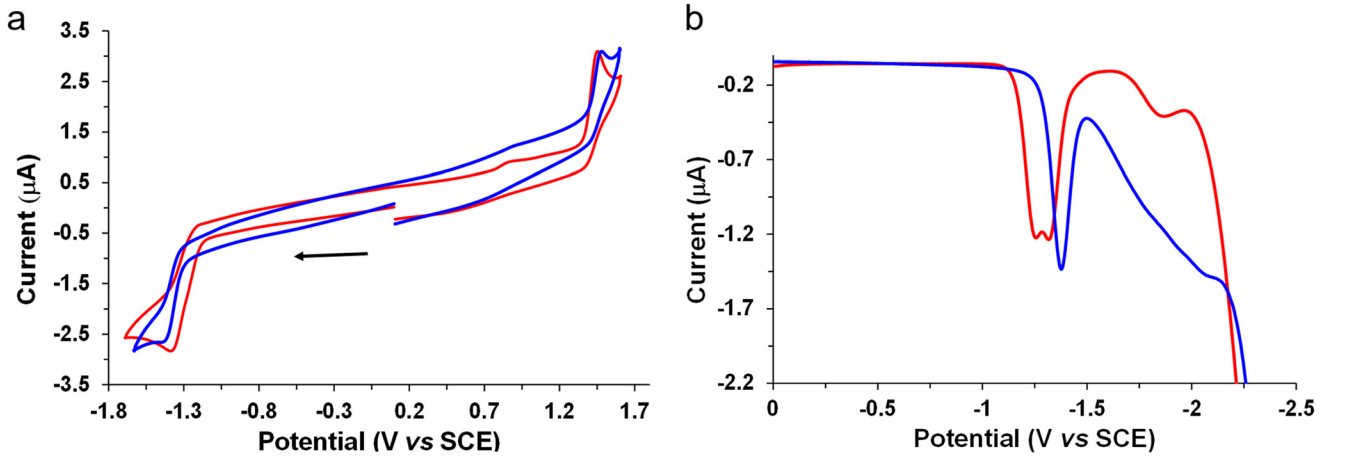

Fig. 6 (a) Cyclic voltammograms of the first oxidation and reduction processes of complexes **Mono-Re-Phe** (2×10^{-3} M, blue line) and **Bi-Re-*para*Phe** (1×10^{-3} M, orange line) at 0.2 V s^{-1} (left); (b) their OSWVs cathodic scans (right) on a Pt working electrode in CH_2Cl_2 + 0.1 M $n[Bu_4N][BF_4]$ at room temperature.

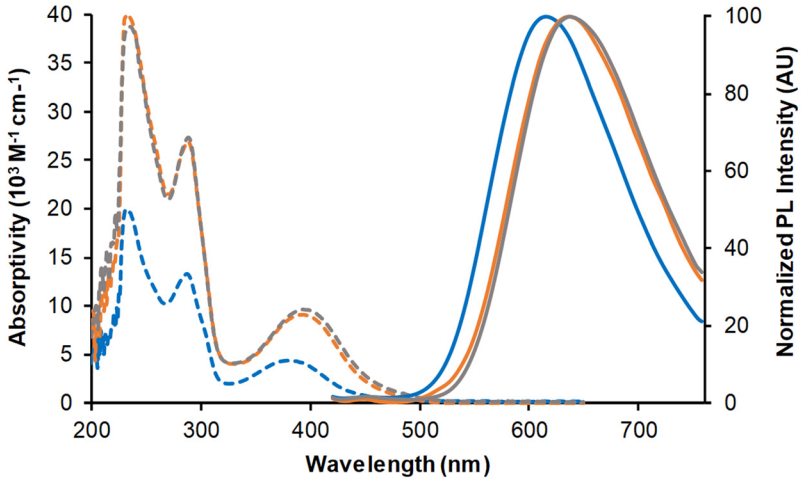

Fig. 7 UV-vis absorption spectra (dotted lines) and normalized emission spectra (solid lines) of complexes **Mono-Re-Phe** (blue lines), **Bi-Re-*para*Phe** (orange lines), and **Bi-Re-*meta*Phe** (grey lines) in aerated dichloromethane. Concentrations: ~5 × 10^{-5} M (monomer) and 2.5 × 10^{-5} M (dimers) for absorption, ~1.1 × 10^{-5} M (monomer) and 5.1 × 10^{-6} M (dimers) for emission. Excitation in the low-energy absorption band.

Table 2 Spectroscopic data of the three complexes in dichloromethane. Maximum absorption wavelength (λ_{abs}), molar extinction coefficient (ε), maximum wavelength of phosphorescence emission (λ_P), emission quantum yield (Φ_P), lifetime (τ) with chi square (χ^2) values. Concentrations: ~5 × 10^{-5} M (monomer) and 2.5 × 10^{-5} M (dimers) for absorption, ~1.1 × 10^{-5} M (monomer) and 5.1 × 10^{-6} M for emission. Emission characteristics in the solid state (pristine and ground powders): photoluminescence maximum wavelength (λ_{PL}), emission quantum yield (Φ_{PL}), and lifetimes (τ_{PL}) with relative amplitude in % (f) and chi square values (χ^2)

	CH_2Cl_2 solutions					Pristine powders			Ground powders			THF-fumed powders	
Compound	λ_{abs} (nm)	ε (M^{-1} cm^{-1})	λ_P (nm)	Φ_P	τ (ns), [χ^2]	λ_{PL} (nm)	Φ_{PL}	τ_{PL} (ns), (f) [χ^2][a]	λ_{PL} (nm)	Φ_{PL}	τ_{PL} (ns), (f) [χ^2][a]	λ_{PL} (nm)	Φ_{PL}
Mono-Re-Phe	232 287 379	20 100 13 400 4400	616	2.1×10^{-2}	114 [1.21]	550	0.37	105 (*2.9*) 1119 (*96.8*) [1.14]	552	0.34	—	—	—
Bi-Re-*para*Phe	231 289 391	40 400 28 000 9900	636	1.4×10^{-2}	72 [1.40]	560	0.27	164 (*11.6*) 934 (*87.8*) [1.16]	582	0.13	229 (*31.1*) 873 (*66.6*) [1.13]	564	0.20
Bi-Re-*meta*Phe	236 289 394	39 000 28 200 9700	638	1.8×10^{-2}	71 [1.39]	552	0.34	195 (*11.5*) 778 (*87.9*) [1.15]	586	0.08	233 (*30.2*) 875 (*67.8*) [1.16]	564	0.15

[a] A short lifetime with weak contribution was also detected. The full data are given in the ESI (Fig. S55 and 56†).

are therefore less sensitive to the presence of dissolved oxygen than their parent complex, which can be explained by their shorter lifetime.

The microcrystalline powders of the **Mono-Re-Phe** and **Bi-Re-*meta*Phe** complexes emitted strong yellow light, with quantum yields up to 0.37 (Table 2 and Fig. 8). The **Bi-Re-*para*Phe** complex emitted ocher light, with slightly lower quantum yield (0.27). In every case, the emission decays were much longer than in solution, indicating strong stabilization of the molecules in the solid state. They also were multiexponential (Fig. S55 and 56†), which reveals the heterogeneity of the microenvironment. The lifetimes associated with preponderant amplitude were just below or above the microsecond range. They could be attributed to bulk molecules. Shorter lifetimes between 100 and 200 ns, with a contribution reaching 11% for the bimetallic complexes, could be assigned to molecules close to the surface or involved in crystal defects. By comparison with solutions, the three complexes therefore show strong SLE effect, mainly due to molecular stiffening in the solid state, which reduces the possibilities of non-radiative deactivation.

Mechanoresponsive luminescence was investigated. To do so, the pristine powders were ground using a mortar and a pestle. Very few emission changes were detected for **Mono-Re-Phe**, as was also the case for **Re-Phe**.[57] In contrast, the dimer ground powders emitted orange light. The red shift of emission was very significant, ranging from 22 nm for **Bi-Re-*para*Phe** to 34 nm for **Bi-Re-*meta*Phe**. Meanwhile, the relative amplitude of the short lifetime was increased with respect to that of the long lifetime, which may indicate the decrease of

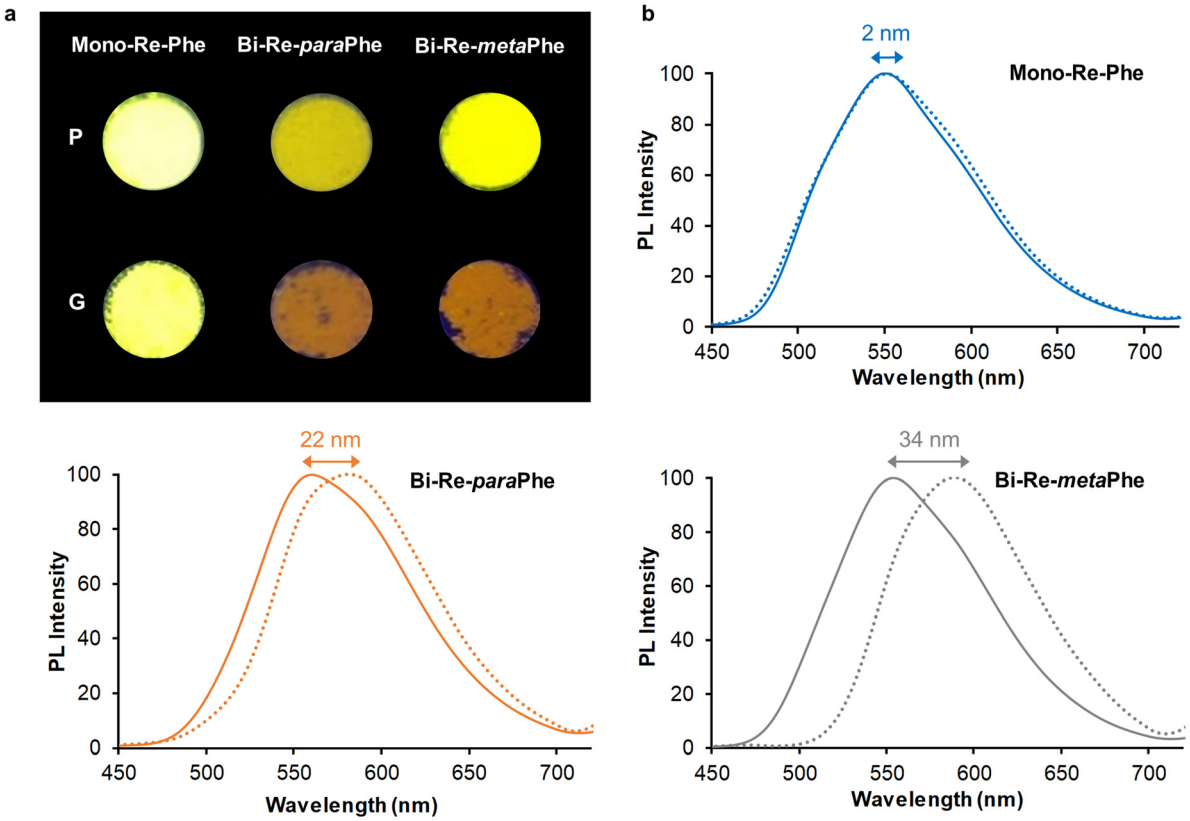

Fig. 8 (a) Image of the pristine and ground powders of the three complexes illuminated by UV light at 365 nm. (b) Normalized photoluminescence spectra of **Mono-Re-Phe** (blue lines), **Bi-Re-*para*Phe** (orange lines), and **Bi-Re-*meta*Phe** (grey lines), as microcrystalline pristine powders (solid lines) and ground powders (dotted lines). The wavelength shift between maxima is indicated. Excitation at 380 nm.

the population of bulk, well-packed molecules. Fuming the ground powders with THF vapors allowed the partial recovery of the initial photoluminescence. The examination of the samples of **Bi-Re-*para*Phe** and **Bi-Re-*meta*Phe** by powder X-Ray diffraction (pXRD) analysis showed that grinding has induced partial amorphization of the pristine microcrystalline sample, and that crystallinity was mostly recovered after THF fuming, which promotes the mobility of molecules (Fig. S57†). A mechanoresponsive luminescence (MRL) behavior thus appears only for dimers, and its amplitude depends on the substitution pattern. For **Bi-Re-*meta*Phe**, it is most likely that the MRL effect is promoted by the loose crystal packing mode and easy sliding of crystalline layers on each other upon grinding. Knowing the crystalline arrangement of **Bi-Re-*para*Phe** would make it possible to say whether this is also the case for this compound.

Finally, it was interesting to see if our three complexes that display strong SLE effect as powders also lead to a valuable aggregation-induced emission (AIE) effect in aqueous medium,[60] knowing that the formation of aggregates in this medium is not always compatible with good light emission. In a very conventional way, the AIE behavior was investigated by increasing the water proportion in an acetonitrile solution of the complexes, which were used at similar concentrations for optimal comparison. For **Mono-Re-Phe**, the weak red emission centered at 624 nm in acetonitrile abruptly became a strong green-yellow emission with maximum at 546 nm when the water fraction reached 90%. Under the same conditions, the red emission of **Bi-Re-*para*Phe** and **Bi-Re-*meta*Phe** at around 628 nm was progressively shifted to the yellow (568 nm) and orange (592 nm) regions, respectively, with a neat increase of intensity (Fig. 9). The intensity of the PL signal at the maximum wavelength of the most intense band was multiplied by 41, 27 and 10, respectively, for **Mono-Re-Phe**, **Bi-Re-*para*Phe** and **Bi-Re-*meta*Phe**. All these spectroscopic changes were accompanied by the appearance of small particles, visible to the naked eye in some samples. The examination under the fluorescence microscope showed for **Mono-Re-Phe** the presence of strongly-emissive rod-like microcrystals, which measured about 10–20 μm × 2 μm and agglomerated. The suspensions of **Bi-Re-*para*Phe** contained numerous yellow-emitting agglomerates of very thin particles. Those of **Bi-Re-*meta*Phe** mainly contained agglomerates of particles that emitted weakly in the orange, together with very rare microcrystals. In the three cases, no particles were clearly visible in the samples containing the highest proportion of water. The red-shifted emission and intensity decrease observed for these samples suggested the formation of possibly amorphous,

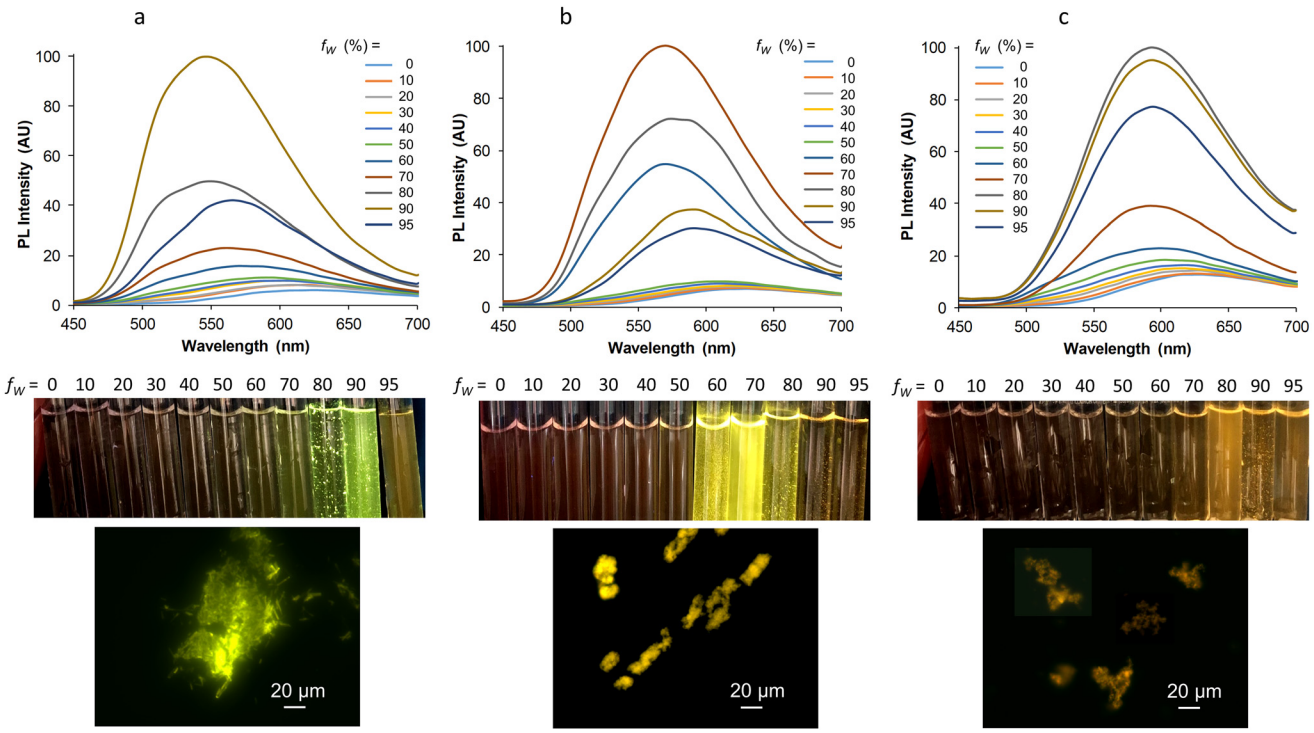

Fig. 9 From top to bottom: emission spectra of **Mono-Re-Phe** (a), **Bi-Re-*para*Phe** (b), and **Bi-Re-*meta*Phe** (c) at ~1.5 × 10^{-5} M in acetonitrile solutions containing from 0 to 95% water, λ_{ex} = 364 nm; corresponding samples illuminated at 365 nm; fluorescence microscopy images of the suspensions at f_w = 80% or 90%. All samples were observed 3 h after preparation.

ultra-small particles. The AIE effect was therefore clear in every case. However, this effect was much shaper for **Mono-Re-Phe**, which appears to be the most suitable complex for AIE-related applications. An explanation could be that the monomer readily gives microcrystals in the presence of water, while the more hydrophobic dimers lead to much smaller particles, where molecules are much less protected from water. Additionally, it is interesting to see that **Bi-Re-*para*Phe** gives a better AIE effect than **Bi-Re-*meta*Phe**, whereas the opposite could have been expected given the examination of the solid-state emission properties of the microcrystalline powders. This indicates that particles formed in contact with water do not necessarily have the same nature as the microcrystals grown in a solvent, and that subsequent interactions with water are difficult to predict.

Conclusion

The three compounds were efficiently synthesized *via* a three-step procedure. In solution, the dinuclear structure was shown to induce minor electronic, electrochemical and spectroscopic variations compared with the mononuclear one. In the solid state, all complexes exhibited clear solid state luminescence enhancement, and significant differences appeared between them. The presence of second metal center did not improve the PL efficiency. The mononuclear derivative even seemed to be more advantageous for applications linked to AIE properties. In contrast, MRL was only observed for the dinuclear complexes. Our previous studies showed that this property appears when replacing chloride by bromide or iodide as ancillary ligands, or introducing a bulky substituent such as an adamantyl or a benzoxazole moiety on the phenyl ring.[56–59] All these complexes form layers in the crystal network, with the inclusion of several solvent molecules. Similarly, the large flat molecules of **Bi-Re-*meta*Phe** organize as a two-dimensional network, thanks to the presence of their alkyl chain and to the crucial role of intermolecular interactions with the solvent. The present work confirms that this type of arrangement is associated with MRL effect. Regarding the influence of regioisomerism, it was observed that the PL efficiency, AIE behavior and the amplitude of the MRL phenomena varied greatly between the two dinuclear complexes. As almost no differences were observed in solution, it can be deduced that those observed in the solid state come from a difference of packing, resulting from the substitution pattern. To the best of our knowledge, the effect of positional isomerism on solid-state emission properties was shown here for the first time.

Our study highlights the potential of dinuclear Re(I) complexes in the field of AIE and MRL-active photoluminescent materials. As the research was limited to just three complexes, expanding the investigation to include a broader range of complexes is necessary to validate these findings. Additionally, exploring other multinuclear structures could provide further

insights. For instance, we have recently shown the interest of mononuclear complexes based on triazolylidene.[55] This type of ligand could easily lead to di-, tri- and tetranuclear complexes.[67,68] We can also learn from relatively close polynuclear tricarbonylmanganese complexes.[69,70] Complexes incorporating four[71] and five[72] tricarbonylrhenium(I) centers, as well as multinuclear Re(I) boxes, some of which have already shown their value for solid-state emission, can also be an endless source of inspiration.[23,73–75]

Experimental section

General methods and synthesis

All purchased chemicals were of the highest purity commercially available and used without further purification. Analytical grade solvents were used as received. Unless otherwise noted, all experiments were carried out under an argon atmosphere. Reactions were monitored by TLC on silica gel Alugram® Xtra SIL G/UV_{254}. Column chromatography was performed on Machery-Nagel silica gel.

NMR, mass and infrared spectra were obtained in the relevant 'Services communs de l'Institut de Chimie de Toulouse, Université de Toulouse III-Paul-Sabatier'. ^{1}H- and ^{13}C-NMR spectra were recorded on Bruker Avance 300 MHz spectrometers. Attributions of the signals were made using 2D NMR data (HSQC and HMBC). Signals are described as follow: bs, broad singlet; s, singlet; d, doublet; t, triplet; q: quadruplet; quint: quintuplet; m, multiplet. App = Apparent. HRMS data were recorded on a Xevo G2 QTOF (Waters) instrument. Fourier transform infrared (FT-IR) spectra were obtained on a Nexus Thermonicolet apparatus with DTGS as the detector. Melting points (Mp) were obtained on a Mettler Toledo apparatus.

2-Octyl-5-(pyridin-2-yl)-1,3,4-oxadiazole (1). A mixture of picolinohydrazide purchased from TCI (1 g, 7.29 mmol), nonanoic acid (1.27 mL, 7.29 mmol), *N*,*N*-diisopropylethylamine (3.79 mL, 21.9 mmol) and *O*-(7-aza-1*H*-benzotriazol-1-yl)-*N*,*N*,*N*′,*N*′-tetramethyluronium hexafluorophosphate (HATU) (3.04 g, 8 mmol) in CH_3CN (45 mL) was stirred at room temperature for 6 h. Then *N*,*N*-diisopropylethylamine (1.26 ml, 7.3 mmol) and *p*-TsCl (2.1 g, 11 mmol) were added to the reaction mixture, which was stirred at room temperature overnight. An ammonia solution (15% in water) was added, the mixture was stirred at room temperature for 15–20 min, and then the aqueous phase was extracted with dichloromethane (DCM). The organic phase was washed with water, dried over anhydrous Na_2SO_4, filtered and evaporated. The crude product was solubilized in DCM, washed with an aqueous solution of NaOH (2 M), and with water. The organic phase was dried over anhydrous Na_2SO_4 and concentrated under reduced pressure. The crude product was purified by chromatography on silica using a mixture of DCM/EtOAc as eluent (gradient from 95 : 5 to 90 : 10 v/v) to give the expected compound **1** (1.56 g, 84% yield) as a brown oil.

^{1}H NMR (300 MHz, $CDCl_3$): δ (ppm) = 8.73 (ddd, 1H, J_{6-5} = 4.8 Hz, J_{6-4} = 1.7 Hz, J_{6-3} = 0.9 Hz, H_6), 8.20 (dt_{app}, 1H, J_{3-4} = 7.9 Hz, $J_{3-5\text{ and }3-6}$ = 1.0 Hz, H_3), 7.84 (td, 1H, $J_{4-3\text{ and }4-5}$ = 7.8, J_{4-6} = 1.7 Hz, H_4), 7.41 (ddd, 1H, J_{5-4} = 7.6 Hz, J_{5-6} = 4.9, J_{5-3} = 1.2 Hz, H_5), 2.92 (t, 2H, J_{8-9} = 7.8 Hz, H_8), 1.83 (quint, 2H, $J_{9-8\text{ and }9-10}$ = 7.5 Hz, H_9), 1.17–1.43 (m, 10H, H_{10}, H_{11}, H_{12}, H_{13}, H_{14}), 0.78–0.86 (m, 3H, H_{15}). ^{13}C NMR (75 MHz, $CDCl_3$): δ (ppm) = 168.2 (C_7), 164.0 (C_1), 150.2 (C_6), 143.8 (C_2), 137.3 (C_4), 125.7 (C_5), 123.0 (C_3), 31.8/29.1/22.7 (C_{10}, C_{11}, C_{12}, C_{13}, C_{14}), 26.6 (C_9), 25.6 (C_8), 14.1 (C_{15}). ESI^+ HRMS *m*/*z* 260.1763 ($[M + H]^+$ calcd for $C_{15}H_{22}N_3O_1$: 260.1763).

2-(5-Octyl-4-phenyl-4*H*-1,2,4-triazol-3-yl)pyridine (L-Phe). A mixture of **1** (300 mg, 1.16 mmol), aniline (126 mg, 1.35 mmol) and *p*-TsOH (26 mg, 0.14 mmol) in 1,2-dichlorobenzene (12 mL) was heated in 180 °C for 20 h. 1,2-Dichlorobenzene was removed under vacuum and the crude product was dissolved in DCM. The organic phase was washed with a NaOH aqueous solution (1 M), dried over anhydrous Na_2SO_4, and concentrated under reduced pressure. The crude product was purified by chromatography on silica using a mixture of EtOAc/MeOH as eluent (gradient from 97 : 3 to 95 : 5 v/v), to afford the expected **L-Phe** ligand as a grey solid (310 mg, 80% yield).

^{1}H NMR (300 MHz, acetone-d_6): δ (ppm) = 8.25 (ddd, 1H, J_{6-5} = 4.8 Hz, J_{6-4} = 1.8 Hz, J_{6-3} = 1.0 Hz, H_6), 8.10 (dt_{app}, 1H, J_{3-4} = 8.0 Hz, J = 1.1 Hz, H_3), 7.87 (td_{app}, 1H, $J_{4-5\text{ and }4-3}$ = 7.8 Hz, J_{4-6} = 1.8 Hz, H_4), 7.52–7.54 (m, 3H, H_b, H_d, H_f), 7.36–7.39 (m, 2H, H_c, H_e), 7.30 (ddd, 1H, J_{5-4} = 7.6 Hz, J_{5-6} = 4.8 Hz, J_{5-3} = 1.2 Hz, H_5), 2.60 (t, 2H, J_{8-9} = 7.8 Hz, H_8), 1.64 (quint, 2H, $J_{9-8\text{ and }9-10}$ = 7.6 Hz, H_9), 1.16–1.35 (m, 10H, H_{10}, H_{11}, H_{12}, H_{13}, H_{14}), 0.84–0.88 (m, 3H, H_{15}). ^{13}C NMR (75 MHz, acetone-d_6): δ (ppm) = 156.3 (C_7), 152.5 (C_2), 148.7 (C_6), 147.8 (C_1), 136.6 (C_4), 136.2 (C_a), 129.1 (C_b, C_f), 128.8 (C_d), 127.7 (C_c, C_e), 123.6 (C_5), 123.3 (C_3), 31.6/28.9/22.4 (C_{10}, C_{11}, C_{12}, C_{13}, C_{14}), 26.9 (C_9), 24.8 (C_8), 13.5 (C_{15}). ESI^+ HRMS *m*/*z* 335.2238 ($[M + H]^+$ calcd for $C_{21}H_{27}N_4$: 335.2236).

General procedure for the preparation of ligands L-*para*Phe and L-*meta*Phe. A mixture of **1** (2.2 eq.), the relevant phenylenediamine (1 eq.) and *p*-TsOH (0.4 eq.) in 1,2-dichlorobenzene was heated in 180 °C for 20 h. 1,2-Dichlorobenzene was removed under vacuum and the crude product was dissolved in DCM. The organic phase was washed with a NaOH aqueous solution (1 M), dried over anhydrous Na_2SO_4, and concentrated under reduced pressure. The crude product was purified by chromatography on silica using a mixture of EtOAc/MeOH as eluent to give the expected pure ligand.

1,4-Bis(3-octyl-5-(pyridin-2-yl)-4*H*-1,2,4-triazol-4-yl)benzene (L-*para*Phe). Following the general procedure, 464 mg (1.79 mmol) of **1**, 88 mg (0.81 mmol) of *p*-phenylenediamine and 62 mg (0.33 mmol) of *p*-TsOH afforded ligand **L-*para*Phe** (288 mg, 60%) as a white solid after chromatography on silica (gradient from 97 : 3 to 90 : 10 v/v).

^{1}H NMR (300 MHz, acetone-d_6): δ (ppm) = 8.32 (ddd, 2H, $J_{6-5\text{ and }6'-5'}$ = 4.8 Hz, $J_{6-4\text{ and }6'-4'}$ = 1.8 Hz, $J_{6-3\text{ and }6-3'}$ = 1.0 Hz, H_6, $H_{6'}$), 8.15 (dt_{app}, 2H, $J_{3-4\text{ and }3'-4'}$ = 8.0 Hz, J = 1.1 Hz, H_3, $H_{3'}$), 7.92 (td_{app}, 2H, $J_{4-5,\ 4-3,\ 4'-5'\text{ and }4'-3'}$ = 7.8 Hz, $J_{4-6\text{ and }4'-6'}$ =

1.8 Hz, H_4, $H_{4'}$), 7.56 (s, 4H, H_b, H_c, H_e, H_f), 7.36 (ddd, 2H, $J_{5-4\text{ and }5'-4'}$ = 7.6 Hz, $J_{5-6\text{ and }5'-6'}$ = 4.8 Hz, $J_{5-3\text{ and }5'-3'}$ = 1.2 Hz, H_5, $H_{5'}$), 2.72 (t, 4H, $J_{8-9\text{ and }8'-9'}$ = 7.7 Hz, H_8, $H_{8'}$), 1.68 (quint, 4H, $J_{9-8,\ 9-10,\ 9'-8'\text{ and }9'-10'}$ = 7.5 Hz, H_9, $H_{9'}$), 1.21–1.40 (m, 20H, H_{10}, H_{11}, H_{12}, H_{13}, H_{14}, $H_{10'}$, $H_{11'}$, $H_{12'}$, $H_{13'}$, $H_{14'}$), 0.81–0.90 (m, 6H, H_{15}, $H_{15'}$). ^{13}C NMR (75 MHz, acetone-d_6): δ (ppm) = 157.2 (C_7, $C_{7'}$), 153.3 (C_2, $C_{2'}$), 149.5 (C_6, $C_{6'}$), 148.5 (C_1, $C_{1'}$), 137.8 (C_4, $C_{4'}$), 137.7 (C_a, C_d), 129.5 (C_b, C_c, C_e, C_f), 124.7 (C_5, $C_{5'}$), 124.2 (C_3, $C_{3'}$), 32.6/30.0/23.4 (C_{10}, $C_{10'}$, C_{11}, $C_{11'}$, C_{12}, $C_{12'}$, C_{13}, $C_{13'}$, C_{14}, $C_{14'}$), 27.9 (C_9, $C_{9'}$), 25.8 (C_8, $C_{8'}$), 14.4 (C_{15}, $C_{15'}$). ESI$^+$ HRMS m/z 591.3930 ([M + H]$^+$ calcd for $C_{36}H_{47}N_8$: 591.3924).

1,3-Bis(3-octyl-5-(pyridin-2-yl)-4*H*-1,2,4-triazol-4-yl)benzene (L-*meta*Phe). Following the general procedure, 467 mg (1.8 mmol) of **1**, 97 mg (0.9 mmol) of *m*-phenylenediamine and 68 mg (0.36 mmol) of *p*-TsOH afforded ligand **L-*meta*Phe** (266 mg, 50%) as an orange solid after chromatography on silica (gradient from 97 : 3 to 90 : 10 v/v).

^{1}H NMR (300 MHz, acetone-d_6): δ (ppm) = 8.29 (bs_{app}, 2H, H_6, $H_{6'}$), 8.15 (d_{app}, 2H, $J_{3-4\text{ and }3'-4'}$ = 7.8 Hz, H_3, $H_{3'}$), 7.90 (t_{app}, 2H, $J_{4-5,\ 4-2,\ 4'-5'\text{ and }4'-2'}$ = 7.8 Hz, H_4, $H_{4'}$), 7.69 (m, 1H, H_e), 7.57 (m, 2H, H_d, H_f), 7.55 (m, 1H, H_b), 7.36 (dd_{app}, 2H, J = 7.0, J = 3.8 Hz, H_5, $H_{5'}$), 2.64 (t, 4H, $J_{8-9\text{ and }8'-9'}$ = 7.5 Hz, H_8, $H_{8'}$), 1.67 (quint, 4H, $J_{9-8,\ 9-10,\ 9'-8'\text{ and }9'-10'}$ = 7.4 Hz, H_9, $H_{9'}$), 1.16–1.35 (m, 20H, H_{10}, H_{11}, H_{12}, H_{13}, H_{14}, $H_{10'}$, $H_{11'}$, $H_{12'}$, $H_{13'}$, $H_{14'}$), 0.83–0.87 (m, 6H, H_{15}, $H_{15'}$). ^{13}C NMR (75 MHz, acetone-d_6): δ (ppm) = 157.3 (C_7, $C_{7'}$), 153.3 (C_2, $C_{2'}$), 149.6 (C_6, $C_{6'}$), 148.5 (C_1, $C_{1'}$), 138.0 (C_a, C_c), 137.8 (C_4, $C_{4'}$), 130.7 (C_e), 129.2 (C_d, C_f), 128.5 (C_b), 124.7 (C_5, $C_{5'}$), 124.2 (C_3, $C_{3'}$), 32.6/30.0/23.4 (C_{10}, C_{11}, C_{12}, C_{13}, C_{14}, $C_{10'}$, $C_{11'}$, $C_{12'}$, $C_{13'}$, $C_{14'}$), 27.7 (C_9, $C_{9'}$), 25.7 (C_8, $C_{8'}$), 14.4 (C_{15}, $C_{15'}$). ESI$^+$ HRMS m/z 591.3924 ([M + H]$^+$ calcd for $C_{36}H_{47}N_8$: 591.3939).

Complex [Re(CO)$_3$(L-*Phe*)Cl] (Mono-Re-Phe). A mixture of ligand **L-Phe** and [Re(CO)$_5$Cl] (1.1 eq.) was stirred in refluxing MeOH for 16 h at 65 °C. The reaction mixture was cooled to room temperature and concentrated under vacuum. The crude product was purified by chromatography on silica using a mixture of DCM/EtOAc as eluent (gradient from 97 : 3 to 95 : 5 v/v), to give **Mono-Re-Phe** as a yellow solid (95 mg, 83% yield).

^{1}H NMR (300 MHz, acetone-d_6): δ (ppm) = 9.11 (ddd, 1H, J_{6-5} = 5.5 Hz, J_{6-4} = 1.6 Hz, J_{6-3} = 0.8 Hz, H_6), 8.04 (td_{app}, 1H, $J_{4-5\text{ and }4-3}$ = 8.0 Hz, J_{4-6} = 1.6 Hz, H_4), 7.84–7.87 (m, 4H, $H_{b/c/e/f}$), 7.74–7.77 (m, 1H, H_d), 7.71 (ddd, 1H, J_{5-4} = 7.8 Hz, J_{5-6} = 5.5 Hz, J_{5-3} = 1.3 Hz, H_5), 6.97 (dt_{app}, 1H, J_{3-4} = 8.1 Hz, J = 1.2 Hz, H_3), 2.66–2.78 (m, 2H, H_8), 1.73 (quint, 2H, $J_{9-8\text{ and }9-10}$ = 7.6 Hz, H_9), 1.20–1.40 (m, 10H, H_{10-14}), 0.84–0.88 (m, 3H, H_{15}). ^{13}C NMR (75 MHz, acetone-d_6): δ (ppm) = 198.2 (CO), 197.3 (CO), 189.0 (CO), 158.9 (C_7), 155.1 (C_2), 154.4 (C_6), 145.3 (C_1), 139.9 (C_4), 132.5 (C_a), 131.8/131.1/127.8 (C_b, C_d, C_e, C_f), 127.5 (C_5), 122.4 (C_3), 31.6/28.8/22.4 (C_{10}, C_{11}, C_{12}, C_{13}, C_{14}), 26.5 (C_9), 24.4 (C_8), 13.5 (C_{15}). ESI$^+$ HRMS m/z 605.1562 [M − Cl]$^+$ calcd for $C_{24}H_{26}N_4O_3Re$: 605.1560. IR (ATR) $\nu_{C\equiv O}$: 2018, 1900, 1886 cm^{-1}. Anal. calcd (%) for $C_{24}H_{26}ClN_4O_3Re$: C 45.03, H 4.09, N 8.75; found: C 46.24, H 4.32, N 8.05.

General procedure for the preparation of dimeric tricarbonylrhenium(I) complexes. A mixture of ligand and [Re(CO)$_5$Cl] (2.2 eq.) was stirred in refluxing methanol for 16 h. The reaction mixture was cooled to room temperature and the yellow precipitate was collected by filtration, washed with MeOH and dried under vacuum. The expected product was pure enough to be used without further purification.

Complex [(Re(CO)$_3$Cl)$_2$(L-*para*Phe)] (Bi-Re-*para*Phe). Following the general procedure, 50 mg (0.085 mmol) of **L-*para*Phe** and 67.3 mg (0.19 mmol) of [Re(CO)$_5$Cl] afforded complex **Bi-Re-*para*Phe** (77 mg, 76% yield) as a yellow solid.

^{1}H NMR (300 MHz, acetone-d_6): δ (ppm) (mixture of isomers): 9.16 (ddd, 2H, $J_{6-5\text{ and }6'-5'}$ = 5.5 Hz, $J_{6-4\text{ and }6'-4'}$ = 1.6 Hz, $J_{6-3\text{ and }6'-3'}$ = 0.8 Hz, H_6, $H_{6'}$), 8.31–8.47 (m, 4H, H_b, H_c, H_e, H_f), 8.25 (td_{app}, 1H, $J_{4/4'-5\text{ and }4/4'-3}$ = 8.0 Hz, $J_{4/4'-6}$ = 1.5 Hz, H_4, $H_{4'}$), 8.06 (td_{app}, 1H, $J_{4/4'-5\text{ and }4/4'-3}$ = 7.9 Hz, $J_{4/4'-6}$ = 1.6 Hz, H_4, $H_{4'}$), 7.75–7.80 (m, 2H, H_5, $H_{5'}$), 7.52–7.55 (m, 1H, H_3, $H_{3'}$), 7.20–7.23 (m, 1H, H_3, $H_{3'}$), 2.78–3.02 (m, 4H, H_8, $H_{8'}$), 1.72–1.91 (m, 4H, H_9, $H_{9'}$), 1.19–1.50 (m, 20H, H_{10}, H_{11}, H_{12}, H_{13}, H_{14}, $H_{10'}$, $H_{11'}$, $H_{12'}$, $H_{13'}$, $H_{14'}$), 0.82–0.89 (m, 6H, H_{15}, $H_{15'}$). ^{13}C NMR (75 MHz, acetone-d_6): δ (ppm) (mixture of isomers): 199.0 (CO), 198.1 (CO), 189.9 (CO), 159.8, 159.7 (C_7, $C_{7'}$), 156.1 (C_1, $C_{1'}$), 155.6, 155.5 (C_6, $C_{6'}$), 146.0, 145.9 (C_2, $C_{2'}$), 141.1, 141.0, 140.6 (C_4, $C_{4'}$), 136.3 (C_d), 132.3, 132.1, 132.0 (C_b, C_c, C_e, C_f), 128.7, 128.6 (C_5, $C_{5'}$), 124.2, 124.1, 123.6 (C_3, $C_{3'}$), 32.6, 30.0, 23.4, 23.3 (C_{10}, C_{11}, C_{12}, C_{13}, C_{14}, $C_{10'}$, $C_{11'}$, $C_{12'}$, $C_{13'}$, $C_{14'}$), 27.5, 27.4 (C_9, $C_{9'}$), 25.6, 25.5 (C_8, $C_{8'}$), 14.4 (C_{15}, $C_{15'}$). ESI$^-$ HRMS m/z 1201.1919 [M − H]$^-$ calcd for $C_{42}H_{45}Cl_2N_8O_6Re_2$: 1201.1932. IR (ATR) $\nu_{C\equiv O}$: 2018, 1907, 1894, 1866 cm^{-1}. Anal. calcd (%) for $C_{42}H_{46}Cl_2N_8O_6Re_2$: C 41.96, H 3.86, N 9.32; found: C 41.81, H 3.40, N 9.21.

Complex [(Re(CO)$_3$Cl)$_2$(L-*meta*Phe)] (Bi-Re-*meta*Phe). Following the general procedure, 60 mg (0.1 mmol) of **L-*meta*Phe** and 81 mg (0.22 mmol) of [Re(CO)$_5$Cl] afforded complex **Bi-Re-*meta*Phe** (89 mg) as a yellow solid (yield 73%).

^{1}H NMR (300 MHz, acetone-d_6): δ (ppm) (mixture of isomers): 9.07–9.15 (m, 2H, H_6, $H_{6'}$), 8.32–8.54 (m, 4H, H_b, H_d, H_e, H_f), 8.21 (td_{app}, 1H, $J_{4/4'-5\text{ and }4/4'-3}$ = 8.0 Hz, $J_{4/4'-6}$ = 1.4 Hz, H_4, $H_{4'}$), 8.13 (dqd, 1H, J = 8.0 Hz, J = 4.2 Hz, J = 1.5 Hz, H_4, $H_{4'}$), 7.69–7.80 (m, 2H, H_5, $H_{5'}$), 7.52–7.58 (m, 1H, H_3, $H_{3'}$), 7.21–7.26 (m, 1H, H_3, $H_{3'}$), 2.74–3.03 (m, 4H, H_8, $H_{8'}$), 1.75–1.85 (m, 4H, H_9, $H_{9'}$), 1.18–1.47 (m, 20H, H_{10}, H_{11}, H_{12}, H_{13}, H_{14}, $H_{10'}$, $H_{11'}$, $H_{12'}$, $H_{13'}$, $H_{14'}$), 0.83–0.90 (m, 6H, H_{15}, $H_{15'}$). ^{13}C NMR (75 MHz, acetone-d_6): δ (ppm) (mixture of isomers): 199.0 (CO), 198.1 (CO), 189.8 (CO), 159.8 (C_7, $C_{7'}$), 156.2, 156.1 (C_1, $C_{1'}$), 155.6, 155.5, 155.4 (C_6, $C_{6'}$), 146.1, 146.0, 145.9 (C_2, $C_{2'}$), 140.9, 140.8, 140.6 (C_4, $C_{4'}$), 135.6, 135.4, 135.3 (C_a, C_c), 135.0, 134.8, 132.7, 132.6, 132.5 (C_b, C_f), 129.6, 129.4, 129.1, 128.8, 128.7 (C_5, $C_{5'}$), 124.0, 123.9, 123.8, 123.7 (C_3, $C_{3'}$), 32.6, 32.5, 30.0, 23.3 (C_{10}, C_{11}, C_{12}, C_{13}, C_{14}, $C_{10'}$, $C_{11'}$, $C_{12'}$, $C_{13'}$, $C_{14'}$), 27.3, 27.2 (C_9, $C_{9'}$), 25.7, 25.6 (C_8, $C_{8'}$), 14.4 (C_{15}, $C_{15'}$). ESI$^-$ HRMS m/z 1197, 1913 ([M − H]$^-$ calcd for $C_{42}H_{45}Cl_2N_8O_6Re_2$: 1197.1898). IR (ATR) $\nu_{C\equiv O}$: 2019, 1937, 1903, 1877 cm^{-1}. Anal. calcd (%) for $C_{42}H_{46}Cl_2N_8O_6Re_2$: C 41.96, H 3.86, N 9.32; found: C 41.00, H 3.62, N 8.94.

Crystallography

Crystallographic data were collected at low temperature (193K) with an Oxford Instruments Cryostream 700+ Series device

using MoK$_\alpha$ radiation (wavelength = 0.71073 Å) on a Bruker AXS D8-Venture diffractometer equipped with a multilayer TRIUMPH X-ray mirror and a Photon III-C14 detector. Phi- and omega-scans were used. The space group was determined on the basis of systematic absences and intensity statistics. An empirical absorption correction was employed.[76] The structures were solved using an intrinsic phasing method (ShelXT).[77] All non-hydrogen atoms were refined anisotropically using the least-square method on F^2.[78] Hydrogen atoms were refined isotropically at calculated positions using a riding model. Selected crystallographic data are collected in Table 3.

Hirshfeld surfaces (HS) were mapped over d_{norm} and shape-index. 3D Hirshfeld surfaces and 2D fingerprint plots (FP)[79] were generated with high resolution based on the crystallographic information file (CIF) using Crystal Explorer 17.5 software.[80] The normalized contact distance (d_{norm}) was defined according to eqn (1), where d_i and d_e are the distances from the surface to the nearest atom interior and exterior to the surface, respectively, and r^{vdw} is the van der Waals radii of the corresponding atoms:

$$d_{norm} = \frac{d_i - r_i^{vdW}}{r_i^{vdW}} + \frac{d_e - r_e^{vdW}}{r_e^{vdW}} \quad (1)$$

On the d_{norm} point representation, intermolecular contacts shorter than the sum of the van der Waals radii ($d_{norm} < 0$) of the interacting atoms are denoted as red spots on the surfaces, whereas longer than the sum of the van der Waals radii ($d_{norm} > 0$) of the interacting atoms are represented by blue regions. The van der Waals contacts ($d_{norm} = 0$) are colored in white. 2D fingerprint plots provide correlation between d_i and d_e.

Powder X-ray diffraction measurements were performed in the LPCNO-INSA laboratory of Toulouse on a Malvern Panalytical Empyrean diffractometer, equipped with a Co anticathode source (wavelength 1.789 Å), a Bragg–Brentano HD primary optics, and a Pixcel1D linear detector. The measurements were made using a monocrystalline silicon sample holder with no background noise. Each diffraction pattern was obtained using a theta-theta symmetric scan with a pitch of 0.02° and an exposure time of 1s per step.

Computational details

The GAUSSIAN16 program package[81] was employed for all calculations (the geometry optimization, the ground-state and excited-state electronic structures, and optical spectra) with the aid of the ChemCraft visualization program.[82] The ground state (S_0), the first excited state (S_1) and the lowest triplet state (T_1) geometries of the complexes were fully optimized with the restricted and unrestricted density functional theory (R-DFT and U-DFT) method using the Perdew–Burke–Ernzerhof PBE1PBE functional with no symmetry constraints.[83] In all calculations, the "double-ζ" quality basis set LANL2DZ with Hay and Wadt's relative effective core potential ECP (outer-core [($5s^2 5p^6$)] electrons and the ($5d^6$) valence electrons)[84,85] was employed for the Re atom. The 6-311+G** basis set for H, C, N and O atoms was used.[86] The solvent effect (dichloromethane, ε = 8.93) was simulated using the Self-Consistent Reaction Field (SCRF) under the Conductor Polarizable Continuum Model (CPCM).[87–89] The vibrational frequencies calculations were performed using the optimized structural parameters of the complexes, to confirm that each optimized structure represents a local minimum on the potential energy surface and all eigenvalues are non-negative. The optimized Cartesian coordinates are included in the ESI part (see Tables S27–38†). On the optimized ground and excited state geometries, the absorption and emission properties were calculated by the time dependent density functional theory (TD-DFT) method at the PBE1PBE/LANL2DZ/6-311+G** level. These methods have

Table 3 Selected crystallographic data of Re(I) complexes **Mono-Re-Phe** and **Bi-Re-*meta*Phe**, and ligands L-***para*Phe** and L-***meta*Phe**

	Mono-Re-Phe	**Bi-Re-*meta*Phe**	**L-*para*Phe**	**L-*meta*Phe**
Empirical formula	$C_{24}H_{26}ClN_4O_3Re$	$C_{42}H_{46}Cl_2N_8O_6Re_2 \cdot 2\ CH_2Cl_2$	$C_{36}H_{46}N_8$	$C_{36}H_{46}N_8 \cdot \frac{1}{2}\ C_3H_6O$
Formula weight	640.15	1372.04	590.81	619.84
Crystal system	Orthorhombic	Monoclinic	Monoclinic	Triclinic
Space group	*Pbca*	*C*2/*c*	$P2_1/n$	$P\bar{1}$
Unit cell dimensions				
a (Å)	11.4066(7)	30.087(2)	20.3002(15)	9.1394(9)
b (Å)	17.3844(10)	12.0833(12)	8.9187(6)	20.290(2)
c (Å)	24.7532(15)	15.2938(15)	20.5373(14)	20.328(2)
α (°)	90	90	90	75.123(4)
β (°)	90	95.995(3)	116.516(3)	79.003(4)
γ (°)	90	90	90	82.681(4)
Volume (Å^3)	4908.5(5)	5529.7(9)	3327.2(4)	3564.1(6)
Z	8	4	4	2
Density (calculated) (Mg m^{-3})	1.732	1648	1.179	1.155
Crystal size (mm^3)	0.200 × 0.040 × 0.040	0.100 × 0.040 × 0.040	0.500 × 0.080 × 0.080	0.200 × 0.200 × 0.020
Reflections collected	200 053	137 719	103 159	102 101
Independent reflections	9826	6392	11 042	17 775
R_{int}	0.0520	0.0646	0.0771	0.0668
Restraints/parameters	233/374	227/375	0/399	889/1089
Final R_1 index $I > 2\sigma(I)$	0.0233	0.0614	0.0620	0.0709
wR_2 (all data)	0.0470	0.1566	0.1798	0.2390
Largest diff. peak and hole (e Å^{-3})	1.020 and −1.072	1.964 and −1.916	0.493 and −0.251	0.490 and −0.393
CCDC	2365135	2365136	2365138	2365137

already shown good agreement with experimental studies for different rhenium(I) complexes.[90]

Electrochemistry

The electrochemical properties of the complexes were determined by cyclic voltammetry (CV) and Osteryoung square wave voltammetry (OSWV) in dichloromethane. The solutions used during the electrochemical studies were typically 1×10^{-3} M in complex, and 0.1 M in supporting electrolyte. The supporting electrolyte $n[Bu_4N][BF_4]$ (Fluka, 99% electrochemical grade) was used as received and simply degassed under Argon. Dichloromethane was dried using an MB SPS-800 solvent purification system just prior to use. The measurements were carried out with an Autolab PGSTAT100 potentiostat controlled by GPES 4.09 software. Experiments were performed at room temperature (r.t.) in a homemade airtight three-electrode cell connected to a vacuum/Ar line. The reference electrode consisted of a saturated calomel electrode (SCE) separated from the solution by a bridge compartment. The counter electrode was a Pt wire of *ca.* 1 cm^2 apparent surface. The working electrode was a Pt microdisk (0.5 mm diameter). Before each measurement, the solutions were degassed by bubbling Ar and the working electrode was polished with a polishing machine (Presi P230). Under these experimental conditions, Fc+/Fc is observed at +0.55 ± 0.01 V *vs.* SCE. OSWVs were obtained using an amplitude of 20 mV, a frequency of 20 Hz, and a step potential of 5 mV.

Spectroscopy

Spectroscopic measurements in solutions were conducted at 20 °C in a temperature-controlled cell. UV-visible absorption spectra and emission spectra in solutions were measured with a Xenius SAFAS spectrofluorometer using cells of 1 cm optical pathway. All emission spectra were corrected. The emission quantum yields in solution (Φ) were determined using the classical formula:

$$\Phi_x = (A_s \times I_x \times {n_x}^2 \times \Phi_s)/(A_x \times I_s \times {n_s}^2) \quad (2)$$

where A is the absorbance at the excitation wavelength, I the integrated emission intensity and n the refractive index. Subscripts s and x refer to the standard and to the sample of unknown quantum yield, respectively. Coumarin 153 (Φ_s = 0.53) in ethanol was used as the standard.[91] The absorbance of the solutions was equal or below 0.06 at the excitation wavelength. The error on the quantum yield values is estimated to be about 10% and 20% for suspensions.

For AIE measurements, a small volume (30 μL) of a concentrated solution of complex in acetonitrile was injected in 2.97 mL of various acetonitrile/water mixtures. The samples were left to stand under stirring in the dark, and then they were sonicated for 5 min before optical measurement, so that they were as homogeneous as possible. Absorbance variations due to scattering by microparticles, and in particular the baseline deviation, were taken into account for measuring the extinction coefficient value, the fluorescence quantum yields of the suspension in the water/acetonitrile 90 : 10 v/v mixture, and the magnitude of the AIE effect.

Solid state spectra were recorded on a HORIBA Fluorolog 3-2iHR320 spectrofluorometer and were corrected. The absolute photoluminescence quantum yield values (Φ_P) were determined using the Xenius SAFAS spectrofluorometer provided with an integrating sphere, by a method based on the one developed by De Mello *et al.*,[92] as described elsewhere.[51] The error was estimated to be about 20%.

The emission decay curves were recorded using the time-correlated single-photon counting (TCSPC) method on the HORIBA Fluorolog 3-2iHR320 spectrofluorometer used at right-angle geometry and equipped with a NanoLED-370 (λ_{ex} = 371 nm). The absorbance of solutions and suspensions at λ_{ex} was lower than 0.1. The solid sample was deposited on a quartz holder. Photons were detected through a monochromator by means of a Hamamatsu R928 photomultiplier. Emission was recorded near the maximum with a bandpass of 10–15 nm. The instrumental response was recorded at 371 nm. All analyses were recorded using the Datastation v2.7 software. The decay curves were analyzed with reconvolution and global non-linear least-squares minimization method using DAS6 v6.8 software. The rate constants for radiative (k_r) and non-radiative (k_{nr}) decay were calculated using the following equation:

$$k_r = \Phi/\tau \text{ and } k_{nr} = (1 - \Phi)/\tau \quad (3)$$

with Φ the emission quantum yield and τ the luminescence lifetime in solution.

Fluorescence microscopy was performed with a Leitz Laborlux D fluorescence microscope equipped with an Andor Luca camera ($\lambda_{ex} \sim$ 450–490 nm, $\lambda_{em} >$ 500 nm).

Author contributions

Stéphen Le Garrec: investigation, writing original draft. David Martins-Bessa: investigation. Mariusz Wolff: investigation, formal analysis, writing original draft. Béatrice Delavaux-Nicot: investigation, writing original draft. Sonia Mallet-Ladeira: investigation. Charles-Louis Serpentini: investigation. Eric Benoist: project administration, funding acquisition, supervision, writing – review and editing. Florence Bedos-Belval: conceptualization, methodology, supervision, writing – original draft. Suzanne Fery-Forgues: conceptualization, methodology, supervision, writing – original draft.

Data availability

The data supporting this article have been included as part of the ESI.† Crystallographic data for compounds **Mono-Re-Phe**, **Bi-Re-*meta*Phe**, **L-*para*Phe** and **L-*meta*Phe** have been deposited at CCDC under numbers 2365135, 2365136, 2365138, 2365137, respectively, and can be obtained from **https://www.ccdc.cam.ac.uk/structures/**.

Conflicts of interest

There are no conflicts to declare.

Acknowledgements

DFT calculations were carried out using resources provided by Wrocław Centre for Networking and Supercomputing (https://www.wcss.wroc.pl), Poland. M. W. thanks Université de Toulouse III for offering him a visiting professor position in September 2023. We are grateful to Mr Nicolas Ratel-Ramond (LPCNO-INSA of Toulouse) for the measurement of powder XRD patterns, and to Dr Alix Sournia-Saquet and Mr Alain Moreau (LCC) for their help in electrochemical measurements.

References

1 L. C.-C. Lee, K.-K. Leung and K. K.-W. Lo, *Dalton Trans.*, 2017, **46**, 16357–16380.
2 R. G. Balasingham, F. L. Thorp-Greenwood, C. F. Williams, M. P. Coogan and S. J. A. Pope, *Inorg. Chem.*, 2012, **51**, 1419–1426.
3 R.-R. Ye, C.-P. Tan, M.-H. Chen, L. Hao, L.-N. Ji and Z.-W. Mao, *Chem. – Eur. J.*, 2016, **22**, 7800–7809.
4 S. A. Sharma, N. Vaibhavi, B. Kar, U. Das and P. Paira, *RSC Adv.*, 2022, **12**, 20264–20295.
5 C. A. Kumar, S. Karthikeyan, B. Varghese, V. Veena, N. Sakthivel and B. Manimaran, *J. Organomet. Chem.*, 2014, **766**, 86e94.
6 B. Ramakrishna, R. Nagarajaprakash, V. Veena, N. Sakthivel and B. Manimaran, *Dalton Trans.*, 2015, **44**, 17629–17638.
7 N. Montesdeoca, R. L. Borkar, M. Sathiyendiran and J. Karges, *Chemistry*, 2024, **30**, 202400217.
8 Z.-Y. Pan, D.-H. Cai and L. He, *Dalton Trans.*, 2020, **49**, 11583–11590.
9 D. Pelleteret, N. C. Fletcher and A. P. Doherty, *Inorg. Chem.*, 2007, **46**, 4386–4388.
10 M.-A. Guillevic, M. E. Light, S. J. Coles, T. Gelbrich, M. B. Hursthouse and D. W. Bruce, *J. Chem. Soc., Dalton Trans.*, 2000, 1437–1445.
11 C. Bruckmeier, M. W. Lehenmeier, R. Reithmeier, B. Rieger, J. Herranz and C. Kavakli, *Dalton Trans.*, 2012, **41**, 5026–5037.
12 R. Giereth, P. Lang, E. McQueen, X. Meißner, B. Braun-Cula, C. Marchfelder, M. Obermeier, M. Schwalbe and S. Tschierlei, *ACS Catal.*, 2021, **11**, 390–403.
13 F.-X. Wang, J.-H. Liang, H. Zhang, Z.-H. Wang, Q. Wan, C.-P. Tan, L.-N. Ji and Z.-W. Mao, *ACS Appl. Mater. Interfaces*, 2019, **11**, 13123–13133.
14 A. B. Solea, G. Demirci, F. M. Harvey, A. Crochet, F. Zobi and O. M. Steiner, *Dalton Trans.*, 2024, **53**, 13743–13755.
15 P. J. Ball, T. Rarog Shtoyko, J. A. Krause Bauer, W. J. Oldham and W. B. Connick, *Inorg. Chem.*, 2004, **43**, 622–632.
16 M. Yu. Petyuk, I. Yu. Bagryanskaya, O. I. Artyushin, V. K. Brel and A. V. Artem'ev, *Mendeleev Commun.*, 2021, **31**, 810–812.
17 M. Yu. Petyuk, A. S. Berezin, I. Yu. Bagryanskaya, O. I. Artyushin, V. K. Brel and A. V. Artem'ev, *Inorg. Chem. Commun.*, 2020, **119**, 108058.
18 P. Cavigli, G. Balducci, E. Zangrando, N. Demitri, A. Amati, M. T. Indelli and E. Iengo, *Inorg. Chim. Acta*, 2016, **439**, 61–68.
19 S. Frantz, M. Sieger, I. Hartenbach, F. Lissner, T. Schleid, J. Fiedler, C. Duboc and W. Kaim, *J. Organomet. Chem.*, 2009, **694**, 1122–1133.
20 N. Saleh, D. Kundu, N. Vanthuyne, J. Olesiak-Banska, A. Pniakowska, K. Matczyszyn, V. Y. Chang, G. Muller, J. A. G. Williams, M. Srebro-Hooper, J. Autschbach and J. Crassous, *ChemPlusChem*, 2020, **85**, 2446–2454.
21 K. S. Kisel, J. R. Shakirova, V. V. Pavlovskiy, R. A. Evarestov, V. V. Gurzhiy and S. P. Tunik, *Inorg. Chem.*, 2023, **62**, 18625–18640.
22 R. Jordan, M. Niazi, S. Schäfer, W. Kaim and A. Klein, *Molecules*, 2022, **27**, 8159.
23 Y. Zhang, M. R. Crawley, C. E. Hauke, A. E. Friedman, T. S. Janik and T. R. Cook, *Eur. J. Inorg. Chem.*, 2017, **34**, 4055–4060.
24 A. Wilting, T. Stolper, R. A. Mata and I. Siewert, *Inorg. Chem.*, 2017, **56**, 4176–4185.
25 L. A. Paul, S. Rajabi, C. Jooss, F. Meyer, F. Ebrahimi and I. Siewert, *Dalton Trans.*, 2020, **49**, 8367–8374.
26 Y. Hayashi, S. Kita, B. S. Brunschwig and E. Fujita, *J. Am. Chem. Soc.*, 2003, **125**, 11976–11987.
27 W. Yang, S. S. Roy, W. C. Pitts, R. L. Nelson, F. R. Fronczek and J. W. Jurss, *Inorg. Chem.*, 2018, **57**, 9564–9575.
28 M. Panigati, M. Mauro, D. Donghi, P. Mercandelli, P. Mussini, L. De Cola and G. D'Alfonso, *Coord. Chem. Rev.*, 2012, **256**, 1621–1643.
29 M. Mauro, C.-H. Yang, C.-Y. Shin, M. Panigati, C.-H. Chang, G. D'Alfonso and L. De Cola, *Adv. Mater.*, 2012, **24**, 2054–2058.
30 X. Xu and H. A. Xiao, *J. Lumin.*, 2012, **132**, 2251–2258.
31 A. W.-T. Choi, K. K.-S. Tso, V. M.-W. Yim, H.-W. Liu and K. K.-W. Lo, *Chem. Commun.*, 2015, **51**, 3442–3445.
32 A. Palmioli, A. Aliprandi, D. Septiadi, M. Mauro and A. Bernardi, *Org. Biomol. Chem.*, 2017, **15**, 1686–1699.
33 M. Proverbio, E. Quartapelle Procopio, M. Panigati, S. Mercurio, R. Pennati, M. Ascagni, R. Leone, C. La Porta and M. Sugni, *Org. Biomol. Chem.*, 2019, **17**, 509–518.
34 F. Palominos, P. Mella, K. Guajardo, G. Günther, A. Vega and N. Pizarro, *Photochem. Photobiol. Sci.*, 2024, **23**, 119–132.
35 J. Muñoz, X. Rojas, F. Palominos, R. Arce, F. Cañas, N. Pizarro and A. Vega, *Polyhedron*, 2023, **239**, 116442.

36 N. P. Liyanage, W. Yang, S. Guertin, S. S. Roy, C. A. Carpenter, R. E. Adams, R. H. Schmehl, J. H. Delcamp and J. W. Jurss, *Chem. Commun.*, 2019, **55**, 993–996.
37 G. Li, Y. Chen, J. Wang, Q. Lin, J. Zhao, L. Jia and H. Chao, *Chem. Sci.*, 2013, **4**, 4426–4433.
38 E. V. Puttock, A. Sil, D. S. Yufit and J. A. G. Williams, *Dalton Trans.*, 2020, **49**, 10463–10476.
39 L. Lu, M. Wang, Z. Mao, T.-S. Kang, X.-P. Chen, J.-J. Lu, C.-H. Leung and D.-L. Ma, *Sci. Rep.*, 2016, **6**, 22458.
40 B. Liu, S. Monro, L. Lystrom, C. G. Cameron, K. Colón, H. Yin, S. Kilina, S. A. McFarland and W. Sun, *Inorg. Chem.*, 2018, **57**, 9859–9872.
41 W. Cheng, R. Sheng, Y. Liu, S. Wang, P. Chen and B. Tong, *Inorg. Chem. Commun.*, 2021, **129**, 108667.
42 M. A. Esteruelas, A. M. López, E. Oñate, A. San-Torcuato, J.-Y. Tsai and C. Xia, *Organometallics*, 2017, **36**, 699–707.
43 E. Martínez-Vollbert, C. Philouze, I. Gautier-Luneau, Y. Moreau, P.-H. Lanoë and F. Loiseau, *Phys. Chem. Chem. Phys.*, 2021, **23**, 24789–24800.
44 P. Alam, C. Climent, P. Alemany and I. R. Laskar, *J. Photochem. Photobiol., C*, 2019, **41**, 100317.
45 L. Ravotto and P. Ceroni, *Coord. Chem. Rev.*, 2017, **346**, 62–76.
46 V. Sathish, A. Ramdass, P. Thanasekaran, K.-L. Lu and S. Rajagopal, *J. Photochem. Photobiol., C*, 2015, **23**, 25–44.
47 L. Ma, Y. Wang, X. Wang, Q. Zhu, Y. Wang, L. Li, H.-B. Cheng, J. Zhang and X.-J. Liang, *Coord. Chem. Rev.*, 2022, **473**, 214822.
48 H. Shen, C. Xu, F. Sun, M. Zhao, Q. Wu, J. Zhang, S. Li, J. Zhang, J. W. Y. Lam and B. Z. Tang, *ChemMedChem*, 2022, **17**, e202100578.
49 V. Sathish, A. Ramdass, Z.-Z. Lu, M. Velayudham, P. Thanasekaran, K.-L. Lu and S. Rajagopal, *J. Phys. Chem. B*, 2013, **117**, 14358–14366.
50 E. Quartapelle Procopio, M. Mauro, M. Panigati, D. Donghi, P. Mercandelli, A. Sironi, G. D'Alfonso and L. De Cola, *J. Am. Chem. Soc.*, 2010, **132**, 14397–14399.
51 J. Gierschner, J. Shi, B. Milián-Medina, D. Roca-Sanjuán, S. Varghese and S. Y. Park, *Adv. Opt. Mater.*, 2021, **9**, 2002251.
52 J. Wang, B. Delavaux-Nicot, M. Wolff, S. Mallet-Ladeira, R. Métivier, E. Benoist and S. Fery-Forgues, *Dalton Trans.*, 2018, **47**, 8087–8099.
53 J. Wang, A. Poirot, B. Delavaux-Nicot, M. Wolff, S. Mallet-Ladeira, J. P. Calupitan, C. Allain, E. Benoist and S. Fery-Forgues, *Dalton Trans.*, 2019, **48**, 15906–15916.
54 A. Poirot, C. Vanucci-Bacqué, B. Delavaux-Nicot, C. Meslien, N. Saffon-Merceron, C.-L. Serpentini, F. Bedos-Belval, E. Benoist and S. Fery-Forgues, *Dalton Trans.*, 2023, **52**, 5453–5465.
55 C. Vanucci-Bacqué, M. Wolff, B. Delavaux-Nicot, A. M. Abdallah, S. Mallet-Ladeira, C.-L. Serpentini, F. Bedos-Belval, K. W. Fong, X. Y. Ng, M. L. Low, E. Benoist and S. Fery-Forgues, *Dalton Trans.*, 2024, **53**, 11276–11294.
56 A. Poirot, C. Vanucci-Bacqué, B. Delavaux-Nicot, N. Saffon-Merceron, C.-L. Serpentini, N. Leygue, F. Bedos-Belval, E. Benoist and S. Fery-Forgues, *Photochem. Photobiol. Sci.*, 2023, **22**, 169–184.
57 A. Poirot, C. Vanucci-Bacqué, B. Delavaux-Nicot, N. Leygue, N. Saffon-Merceron, F. Alary, F. Bedos-Belval, E. Benoist and S. Fery-Forgues, *Dalton Trans.*, 2021, **50**, 13686–13698.
58 A. Poirot, N. Leygue, B. Delavaux-Nicot, N. Saffon-Merceron, C. Allain, E. Benoist and S. Fery-Forgues, *J. Photochem. Photobiol., A*, 2023, **445**, 114982.
59 J. P. Calupitan, A. Poirot, J. Wang, B. Delavaux-Nicot, M. Wolff, M. Jaworska, R. Métivier, E. Benoist, C. Allain and S. Fery-Forgues, *Chem. – Eur. J.*, 2021, **27**, 4191–4196.
60 H. Shen, C. Xu, F. Sun, M. Zhao, Q. Wu, J. Zhang, S. Li, J. Zhang, J. W. Y. Lam and B. Z. Tang, *ChemMedChem*, 2022, **17**, e202100578.
61 V. W.-W. Yam, Y. Yang, J. Zhang, B. W.-K. Chu and N. Zhu, *Organometallics*, 2001, **20**(23), 4 11–4918.
62 O. S. Wenger, L. M. Henling, M. W. Day, J. R. Winkler and H. B. Gray, *Inorg. Chem.*, 2004, **43**, 2043–2048.
63 M. A. Spackman and D. Jayatilaka, *CrystEngComm*, 2009, **11**, 19–32.
64 W. Kaim and S. Kohlmann, *Inorg. Chem.*, 1990, **29**, 2909–2914.
65 S. Frantz, M. Sieger, I. Hartenbach, F. Lissner, T. Schleid, J. Fiedler, C. Duboc and W. Kaim, *Organomet. Chem.*, 2009, **694**, 1122–1133.
66 R. Jordan, M. Niazi, S. Schäfer, W. Kaim and A. Klein, *Molecules*, 2022, **27**, 8159.
67 E. B. Patricio-Rangel, V. Salazar-Pereda, O. Cortezano-Arellano and D. Mendoza-Espinosa, *Dalton Trans.*, 2022, **51**, 2641–2651.
68 Á. Vivancos, C. Segarra and M. Albrecht, *Chem. Rev.*, 2018, **118**, 9493–9586.
69 I. Mishra, M. Priyatharsini and M. Sathiyendiran, *J. Organomet. Chem.*, 2021, **949**, 121934.
70 P. Govender, S. Pai, U. Schatzschneider and G. S. Smith, *Inorg. Chem.*, 2013, **52**, 5470–5478.
71 U. Phukon, M. Priyatharsini and M. Sathiyendiran, *J. Organomet. Chem.*, 2020, **923**, 121460.
72 R. Xu, X.-S. Wang, H. Zhao, H. Lin, Y.-B. Huang and R. Cao, *Catal. Sci. Technol.*, 2018, **8**, 2224–2230.
73 B.-C. Tzeng, Y.-J. Hsiao, G.-H. Lee, H.-Y. Wang, C. F. Leong, D. M. D'Alessandro and J.-L. Zuo, *Dalton Trans.*, 2019, **48**, 7946–7952.
74 B. Manimaran, P. Thanasekaran, T. Rajendran, R.-T. Liao, Y.-H. Liu, G.-H. Lee, S.-M. Peng, S. Rajagopal and K.-L. Lu, *Inorg. Chem.*, 2003, **42**, 4795–4797.
75 G.-X. Jin, T. Wang, Y. Sun, Y.-L. Li and J.-P. Ma, *Inorg. Chem.*, 2020, **59**, 15019–15027.
76 *SADABS, Program for data correction*, Bruker-AXS.
77 G. M. Sheldrick, *Acta Crystallogr., Sect. A: Found. Adv.*, 2015, **71**, 3–8.
78 G. M. Sheldrick, *Acta Crystallogr., Sect. C: Struct. Chem.*, 2015, **71**, 3–8.
79 M. A. Spackman and J. J. McKinnon, *CrystEngComm*, 2002, **4**, 378–392.

80 P. R. Spackman, M. J. Turner, J. J. McKinnon, S. K. Wolff, D. J. Grimwood, D. Jayatilaka and M. A. Spackman, *J. Appl. Crystallogr.*, 2021, **54**, 1006–1011.
81 M. J. Frisch, G. W. Trucks, H. B. Schlegel, G. E. Scuseria, M. A. Robb, J. R. Cheeseman, G. Scalmani, V. Barone, B. Mennucci, G. A. Petersson, H. Nakatsuji, M. Caricato, X. Li, H. P. Hratchian, A. F. Izmaylov, J. Bloino, G. Zheng, J. L. Sonnenberg, M. Hada, M. Ehara, K. Toyota, R. Fukuda, J. Hasegawa, M. Ishida, T. Nakajima, Y. Honda, O. Kitao, H. Nakai, T. Vreven, J. A. Montgomery, J. E. Peralta, F. Ogliaro, M. Bearpark, J. J. Heyd, E. Brothers, K. N. Kudin, V. N. Staroverov, R. Kobayashi, J. Normand, K. Raghavachari, A. Rendell, J. C. Burant, S. S. Iyengar, J. Tomasi, M. Cossi, N. Rega, J. M. Millam, M. Klene, J. E. Knox, J. B. Cross, V. Bakken, C. Adamo, J. Jaramillo, R. Gomperts, R. E. Stratmann, O. Yazyev, A. J. Austin, R. Cammi, C. Pomelli, J. W. Ochterski, R. L. Martin, K. Morokuma, V. G. Zakrzewski, G. A. Voth, P. Salvador, J. J. Dannenberg, S. Dapprich, A. D. Daniels, O. Farkas, J. B. Foresman, J. V. Ortiz, J. Cioslowski and D. J. Fox, *Gaussian 09, Revision A.1*, Gaussian, Inc., Wallingford CT, 2009.
82 G. Zhurko and D. Zhurko, *ChemCraft 1.6*, 2011, **https://www.chemcraftprog.com/index.html**.
83 J. P. Perdew, K. Burke and M. Ernzerhof, *Phys. Rev. Lett.*, 1996, **77**, 3865–3868.
84 P. J. Hay and W. R. Wadt, *J. Chem. Phys.*, 1985, **82**, 270–283.
85 P. J. Hay and W. R. Wadt, *J. Chem. Phys.*, 1985, **82**, 299–310.
86 W. J. Hehre, L. Radom, P. V. R. Schleyer and J. A. Pople, *Ab initio Molecular Orbital Theory*, Wiley, New York, 1986.
87 V. Barone and M. Cossi, *J. Phys. Chem. A*, 1998, **102**, 1995–2001.
88 M. Cossi, N. Rega, G. Scalmani and V. Barone, *J. Comput. Chem.*, 2003, **24**, 669–681.
89 J. Tomasi, B. Mennucci and R. Cammi, *Chem. Rev.*, 2005, **105**, 2999–3094.
90 G. Velmurugan, B. K. Ramamoorthi and P. Venuvanalingam, *Phys. Chem. Chem. Phys.*, 2014, **16**, 21157–21171.
91 K. Suzuki, A. Kobayashi, S. Kaneko, K. Takehira, T. Yoshihara, H. Ishida, Y. Shiina, S. Oishi and S. Tobita, *Phys. Chem. Chem. Phys.*, 2009, **11**, 9850–9860.
92 J. C. De Mello, H. F. Wittmann and R. H. Friend, *Adv. Mater.*, 1997, **9**, 230–232.